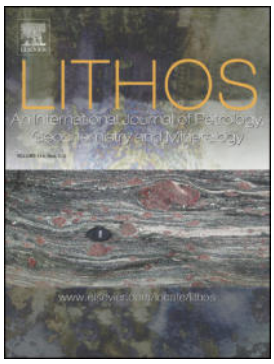

Differential platinum group elements (PGE) re-mobilization at low fS2 in Abdasht and Soghan mafic-ultramafic complexes (Southern Iran)

Grieco Giovanni, Bussolesi Micol, Eslami Alireza, Gentile Andrea, Cavallo Alessandro, Lian Dongyang, Yang Jingsui, Ghaseminejad Farhad

PII: S0024-4937(20)30161-4

DOI: https://doi.org/10.1016/j.lithos.2020.105523

Reference: LITHOS 105523

To appear in: *LITHOS*

Received date: 5 December 2019

Revised date: 30 March 2020

Accepted date: 3 April 2020

Please cite this article as: G. Giovanni, B. Micol, E. Alireza, et al., Differential platinum group elements (PGE) re-mobilization at low fS2 in Abdasht and Soghan mafic-ultramafic complexes (Southern Iran), *LITHOS* (2020), https://doi.org/10.1016/j.lithos.2020.105523

Differential Platinum Group Elements (PGE) re-mobilization at low fS_2 in Abdasht and Soghan mafic-ultramafic complexes (Southern Iran)

[a*]Grieco Giovanni, [a]Bussolesi Micol, [b]Eslami Alireza, [a]Gentile Andrea, [c]Cavallo Alessandro, [d]Lian Dongyang, [d]Yang Jingsui, [e]Ghaseminejad Farhad

[a] Department of Earth Sciences, University of Milan, via S. Botticelli 23, 20133, Milan, Italy

[b] ISTerre, Maison des Géosciences, Université de Grenoble I, CNRS, Grenoble, France

[c] Department of Earth and Environmental Sciences – DISAT, University of Milan-Bicocca, p.zza della Scienza 1–4, 2016, Milan, Italy.

[d] School of Earth Science and Engineering, Nanjing University, Nanjing, China, 210023

[e] Department of Geology, Faculty of Science, University of Isfahan, Isfahan, 8174673441, Iran

* Corresponding Author: Giovanni Grieco, e-mail: giovanni.grieco@unimi.it

Abstract

The Abdasht and Soghan ultramafic complexes, Southern Iran, host major actively exploited chromitite bodies, variably enriched in PGE. The Platinum Group Minerals (PGM) –– Base Metal Minerals (BMM) assemblage was studied in order to assess PGE remobilization during post-magmatic processes. Studied chromitites have variable textures: massive, banded, nodular and disseminated. Primary silicates are almost completely replaced by serpentine. Ferrian chromitization is present but not widespread. BMM are mostly found in the silicate matrix, while PGM are more common as inclusions within chromites.

Primary BMM (pentlandite and bornite) within the silicate matrix are poorly preserved, while primary PGM (laurite) are more abundant. Secondary BMM (heazlewoodite, millerite and Ni-Fe alloys) and PGM (PGE-alloys) are the dominant mineralogical species. During serpentinization the pervasive percolation of low fS_2 fluids induced the desulfurization of the metallic assemblage. Primary sulfides were replaced by S-poor (heazlewoodite) or S-free (Ni-Fe alloys, PGE alloys, PGE-BM alloys) phases.

Low fS_2 differentially mobilized PGE. The release of IPGE (Ir, Os, Ru) into the fluids follows the order: Ru>>Os>Ir. PPGE (Pt, Pd, Rh) mobility is more difficult to assess, due to their small concentration, but the evidence suggests that Rh is more mobile than Ru, and that Pd and Pt were partially added to the system by

fluids. A mass balance calculation on a polyphasic grain, showing differential stages of desulfurization, allowed a semi-quantitative analysis on the desulfurization degree of Abdasht and Soghan complexes, estimated, in the more serpentinized portions, between 75 and 100%.

Keywords: Abdasht-Soghan complex, chromitites, platinum-group elements, platinum-group minerals, desulfurization, Iran

1. Introduction

Chromium is a highly refractory lithophile element. Its concentration in the mantle is similar to the one of the CI model and about 20 times the one in the continental crust (McDonough and Sun, 1995). Platinum Group Elements (PGE) are also highly refractory and show siderophile and chalcophile affinity (Fleet et al., 1999; Lorand et al., 2008; Mungall and Naldrett, 2008; Righter, 2003). During the early stages of Earth differentiation, due to their Fe affinity, they mostly partitioned into the core (O'Neill et al., 1995); their concentration in the mantle is about 10^5 times lower than in the CI model, but still 10^2 times higher than in the continental crust (Lorand et al., 2008; McDonough and Sun, 1995; Wedepohl et al., 1995). High concentrations of Cr and PGE in the mantle, compared to continental crust, together with their refractory behavior can explain why they are enriched in igneous rocks derived by crystallization from primitive melts. Chromitites may contain high concentrations of Platinum Group Elements, usually in the range of 10^2 – 10^3 ppb for the sum of all 6 PGE (e.g. Andrews and Brenan, 2002; Economou, 1986; Gervilla et al., 2005; González-Jiménez et al., 2014; Prichard and Lord, 1988; Zaccarini et al., 2016). PGE chondritic patterns of podiform chromitites show a relative enrichment in Os, Ru and Ir, and a depletion in Pt, Pd and Rh. This is reflected by IPGE-enriched PGM, commonly found as inclusions in chromites or, less frequently, within the associated silicates (González-Jiménez et al., 2011; Prichard et al., 1986). Apart of PGM, PGE can be present in solution within BMM (Ahmed, 2007; Ballhaus and Ryan, 1995; González-Jiménez et al., 2009; Stockman and Hlava, 1984; Tredoux et al., 1995; Wirth et al., 2013). The common euhedral shape of PGM included in chromite suggests a precipitation from a magma. Experiments prove the stability of laurite up to 1275 °C at log(fS_2) of -2. At higher temperatures laurite is replaced by a Ru alloy (Brenan and Andrews, 2001). At log(fS_2) between -2 and -1.3, and T<1260 °C the coexistence of laurite with Ru-Os-Ir alloys was observed (Brenan and Andrews, 2001). However, some Authors argue for a late to post magmatic origin of

PGE alloys in chromitites (Brenker et al., 2003; Garuti and Zaccarini, 1997; González-Jiménez et al., 2011; González-Jiménez et al., 2014; Prichard et al., 2008). This second interpretation of the formation of PGE alloys is supported by evidence related to shape and textural position of these minerals within the host rock. When PGM grains are found associated to fractures and pores, it is possible to find partially desulfurized laurites (González-Jiménez et al., 2010; Proenza et al., 2007; Stockman and Hlava, 1984; Torres-Ruiz et al., 1996; Zaccarini et al., 2005), or completely desulfurized crystals replaced by PGE alloys, arsenides, antimonides and sometimes oxides with irregular shapes (Garuti and Zaccarini, 1997; Prichard et al., 2008). The formation of alloys after primary sulfides is interpreted as a small-scale PGE remobilization due to circulation of serpentinizing fluids (Garuti and Zaccarini, 1997; Proenza et al., 2007). González-Jiménez et al. (2010) state that alteration of primary PGM sulfides implies the dissolution of the grain boundaries due to S loss, and in some cases remobilization of Ru and Os.

Stability of PGM and PGE partition coefficients between PGM and fluids in a wide range of temperature conditions in-between magmatic and ambient environments are poorly known. Little is known also about the factors affecting PGE re-mobilization in this wide range of temperatures, such as fS_2 and fO_2 of the fluid phase and textural position of PGM in the rock assemblage, and about the extent and distance at which remobilization can occur.

Chromitites of the Abdasht-Soghan massif provide a good case-study of PGE remobilization during post-magmatic processes. These rocks underwent extensive interaction with metamorphic fluids that caused differential remobilization of PGE. Understanding the behavior of PGE helps discriminating between primary (magmatic) and secondary (post-magmatic) features of PGE mineralizations. Post-magmatic PGE differential remobilization could affect PGE chondritic patterns and ratios, often used to infer primary features of the rock. Post-magmatic, fluid-mediated, alteration could also lead to the formation of secondary, structurally controlled, PGE mineralization.

2. Geological Setting

The Haji Abad-Esfandagheh district of Kerman province, Southern Iran, is located in a very tectonically active zone, composed of Sanandaj–Sirjan/Bajgan–Durkan highly deformed metamorphic rocks with Early Paleozoic or older in age (McCall, 1985) which are covered by highly deformed and disrupted Carboniferous

to Lower Paleocene platform sequences, coloured mélange and several mafic–ultramafic complexes (Fig. 1a). Soghan and Abdasht mafic-ultramafic complexes as well as Sikhoran, Colkahan and other complexes are situated in a 60 km long and 5-10 km wide E-W trending area in this district (Jannessary et al., 2012; Najafzadeh and Ahmadipour, 2016). Soghan and Abdasht are considered part of the inner belt of the Zagros Mesozoic ophiolites, with an age spanning from Late Triassic to Cretaceous. Haji-Abad-Esfandagheh complexes are the second largest chromite producers in Iran after the Faryab chromitite deposits.

2.1. Abdasht complex

Abdasht complex, that extends for 7×5 km in N–S and E–W directions respectively, is located about 3 km west of Soghan. It is mainly composed of variably serpentinized dunite, harzburgite, websterite and minor wherlite and lherzolite (Fig. 1b). Harzburgite is the most abundant rock type exposed within the complex (Najafzadeh and Ahmadipour, 2016). Dunites, occurring as small pods, elongated lenses and relatively extended deformational layers, show sharp contacts with host harzburgites. (Najafzadeh and Ahmadipour, 2016). According to Jannessary et al. (2012) there are several chromitite ore bodies in the Abdasht complex that follow three distinct pseudo-stratigraphic levels. The ore bodies extend for a total of more than 3 km, and only some of them are actively exploited. These chromitite bodies are included in mantle tectonite (dunites and harzburgites) and have different textures including schlieren/disseminated in the basal level, tabular/disseminated in the intermediate level and layered/massive in the highest level. Jannessary et al. (2012) ascribed this succession of ore types to the upper parts of the mantle tectonite zone, probably close to the transition zone towards the base of cumulates. According to Najafzadeh and Ahmadipour (2016), all chromitite ore bodies are concordant with the host rock layering. The boundaries between chromitites and dunites are commonly well defined.

2.2. Soghan complex

Soghan complex is about 8 and 5 km in N–S and E–W directions respectively and is composed of five main units (Fig 1c): the Gechin unit, the Main Soghan unit, the Transition Zone and Layered Gabbros, overlain by Sargaz-Abshur metamorphic unit.

Gechin unit is located in the northern portion of the complex, with fault contact both with coloured mélange zone and with the Main Soghan unit. This unit is composed of strongly serpentinized dunite and harzburgite.

Minor chromitite massive ores as chromitite lens-shaped bodies were exploited in past (Gechin mine). Layering has been largely obliterated by several thrust faults. The Main Soghan unit is characterized by alternating dunite, harzburgite, and chromitite, which are highly faulted and metamorphosed. The peridotites underwent strong degrees of serpentinization. Main Soghan unit is cross-cut by several diabasic dykes up to few meters thick (Ahmadipour et al., 2003). The unit hosts most of the chromitite ore bodies of the Soghan massif. Chromitite textures are disseminated, banded, schlieren, nodular and massive. Transition Zone crops out to the south-east of the Main Soghan unit with thickness ranging from 50 to 600 m. This unit is characterized by well-bedded lherzolite, dunite, pyroxenite and wherlite (Ahmadipour et al., 2003). Ultramafic rocks underwent various degrees of serpentinization. Layered Gabbro forms the southeastern part of the Soghan complex and is intruded into Sargaz-Abshur metamorphic unit. In Main Soghan unit peridotites dykes are concentrated in the southeastern part. They exhibit quenched margins and intruded parallel to the peridotite compositional layering (N60/80SE) (Ahmadipour et al., 2003). K-Ar age dating of diabasic dykes yields an age of 76+4.5 Ma, in Late Cretaceous time, thus, they represent the last magmatic phase in this complex.

Soghan, and especially Abdasht complexes, are not extensively studied, and the context and timing of their genesis is controversial. Sabzehei (1974) firstly considered mafic-ultramafic units of Esfandagheh district as a part of Sanandaj-Sirjan metamorphic zone and suggested that Soghan complex derived from differentiation of a tholeiitic magma similar to those of other mafic-ultramafic associations in the area. Sabzehei (1998) and Ahmadipour et al. (2003) inferred that Soghan complex represents a mantle diapir emplaced and formed from differentiation of a huge mass of ultramafic (komatiitic) magma in Upper Proterozoic-Lower Paleozoic in an intracontinental rift basin. This interpretation could be therefore inferred for other nearby mafic-ultramafic complexes (Abdasht, Sikhuran) which show similar petrological features. Najafzadeh and Ahmadipour (2014) suggested that Soghan chromitites were possibly formed by fore-arc related magma with boninitic affinity under low oxygen fugacity conditions. Najafzadeh and Ahmadipour (2016) suggested similar genesis for the Abdasht chromitites.

3. Analytical methods

Samples used in this study were collected during field work in Abdasht and Soghan massifs conducted by the Authors. A total of 24 samples were taken from surface outcrops, from stocks of ore, and in underground galleries. All sampling localities were active or abandoned chromite mines. They comprised Panjāh Metri, Omid Bekhoda and Gechin Mines from Soghan massif and two different sites, Main site and Momtaz, of Abdasht Mine from Abdasht massif.

Samples were chosen in order to be representative of all chromitite textures and of their host dunites. Chromitite sampled textures included disseminated, banded, nodular, fine and coarse-grained massive chromitites and some host rocks, mostly dunites.

All samples were examined in transmitted and reflected light optical microscopes. Mineral chemistry was determined with a JEOL 8200 electron microprobe equipped with a wavelength dispersive system (SEM-WDS) at the Earth Sciences Department of the University of Milan. The system was operated using an accelerating voltage of 15kV, a sample current on brass of 15nA, a counting time of 20s on the peaks and 10s on the background. Ka lines were used for major elements, and Ma lines for PGM analyses. A series of natural minerals were used as standards for chromite analyses: wollastonite for Si, forsterite for Mg, ilmenite for Ti, fayalite for Fe, anorthite for Al and Ca, chromite for Cr and niccolite for Ni. The approximate detection limit is 0.01 wt% for each element. For the analyses of PGM and BMM, PGM standards used are niccolite for As and Ni, chalcopyrite for S, Fe, Cu and pure metals for Os, Ir, Rh, Pt, Pd, and Ru.

Platinum-group elements (PGE) were concentrated using the nickel sulfide fire assay and Te-coprecipitation method (Jackson et al., 1990), and were analyzed using ICP-MS at the National Research Center for Geoanalysis, Chinese Academy of Geological Sciences, Beijing. PGE reference material GBW07290 was measured to ensure consistency of the analytical results for PGE. Analytical processes have been described in detail by Dai et al. (2011).

4. Mineralogy and texture

4.1. Main assemblage

Chromitites from the Abdasht-Soghan complex are mostly composed of subhedral to anhedral crystals of chromian spinel in an olivine-serpentine-chlorite groundmass. The size of the grains is highly variable,

ranging from few micrometers in dunites with disseminated chromite, up to 10 mm in massive and coarse nodular chromitites. Nearly all the samples are little- to highly-fractured, testifying that this rock underwent a strong deformation process.

The most common textures are fine to coarse-grained massive and banded chromitites, while nodular texture is less common. Disseminated chromitites are widespread as low grade ore surrounding the main massive and banded ore bodies.

Fe-chromite alteration is present but it affects chromite grains at very different degrees. While some samples are virtually Fe-chromite free, in other samples all chromite grains are partially transformed into Fe-chromite, mainly at rims and along fractures. The extent of Fe-chromitization is well outlined by the high porosity of Fe-chromite compared to the low porosity of primary chromite and can reach up to 60 % in massive and banded chromitites and up to 100 % in disseminated ones.

Phases included in primary chromite are olivine, serpentine, rutile, ilmenite and PGM. Less common are the primary inclusions of Base Metal Minerals (BMM). Pores in Fe-chromites can host serpentine or chlorite.

Primary phases in the gangue of chromitites are very rare and limited to few partially altered olivine relics. Only a few samples of dunites from Soghan massif show a lower degree of serpentinization and abundant olivine. The most common secondary phase is serpentine that replaces olivine, developing from fractures. Small magnetite grains are systematically associated to serpentine. Cr-chlorite is widespread but unevenly distributed and always grows over serpentine. It is absent in some samples, abundant in other ones and can completely replace serpentine in some cases. The abundance of Cr-chlorite is systematically positively correlated to the degree of Fe-chromitization. Brucite and Mg-Fe-hydroxides are sometimes present and abundant in a couple of samples (Fig. 2). Dolomite was detected as a minor late phase at Omid Bekhoda Mine and late uvarovite crystals were found in samples from Gechin Mine.

4.2. Sulfides

Grains, blebs, and aggregates of BMM were found mainly in the silicate matrix and more rarely as small inclusions within chromite. BMM are abundant in all samples from Abdasht massif, while Soghan massif is characterized by a lower amount and diversity.

In the Soghan samples, the BMM assemblage is dominated by heazlewoodite and awaruite, with the second one more abundant, and, where both are present, the latter systematically replaces the former (Fig. 3A).

The only primary sulfide found is a pentlandite grain rimmed by bornite. Cu was also found as native Cu forming a 20 microns irregular bleb between Fe-chromite and Cr-chlorite (Fig. 3B).

In Abdasht massif the BMM assemblage is more diversified than in Soghan. Like in Soghan the only primary sulfide is pentlandite that is anyway very rare. The most abundant secondary phase is heazlewoodite, but maucherite is also quite common, providing an As signature absent in Soghan. Late millerite can replace either maucherite or heazlewoodite (Fig. 3C). The only Cu phase found in Abdasht is a Ni-Cu alloy within a PGM-BMM aggregate, where the other BMM is heazlewoodite (Fig. 4C).

4.3. PGM

A total of twenty PGM were found in the studied sections, but some of them could not be analyzed due to their small size. Ru-rich laurite-erlichmanite solid solution is the most abundant PGM species, always included in chromite, as euhedral crystals (Fig. 4A), multiphase silicate-laurite assemblage (Fig. 4B) and polyphasic PGM or PGM/BMM aggregates (Fig. 4C).

Other PGM detected were mostly PGE alloys. They also are always included in chromite, but systematically associated to pores or fractures. They can be found as single grain inclusions (Fig. 5A), or as rims partially substituting laurite, with (Fig. 5B) or without (Fig. 5C) reaction zones. The only other PGM detected are cuproiridsite and chengdeite.

5. Mineral chemistry

Representative analyses of chromite and BMM are reported in Table 1 and Table 2, respectively. Analyses of PGM are reported in Table 3.

5.1. Chromite

Chromite composition is homogeneous between the two massifs. Compositional variations are present only between unaltered and altered chromite, and in different chromite textures.

Unaltered chromites show an average Cr# [Cr/(Cr+Al)] of 0.77, an average Mg# [Mg/(Mg+Fe^{2+})] of 0.66 and an average Fe^{3+}# [Fe^{3+}/(Fe^{2+}+Mg+Al)] of 0.07. TiO_2 values are low, averaging 0.14 wt%, and Al_2O_3 average content is 11.60 wt%.

Some differences occur in chromite mineral chemistry depending on the rock texture. In fine- and coarse-grained massive chromitites chromite Cr# ranges from 0.67 to 0.83 (with average of 0.78), Mg# from 0.61 to 0.75 (with average of 0.68) and Fe^{3+}# is lower than 0.10 (with average of 0.06). Banded chromitites have Cr# ranging from 0.77 to 0.83 (with average of 0.80), Mg# from 0.58 to 0.72 (with average of 0.66) and Fe^{3+}# from 0.04 to 0.09 (with average of 0.08). Disseminated chromites Cr# ranges from 0.63 to 0.65 (with average of 0.64), Mg# from 0.53 to 0.56 (with average of 0,55) and Fe^{3+}# from 0.04 to 0.05 (with average of 0.04). In nodular chromitite, chromites Cr# ranges from 0.73 to 0.80 (with average of 0.77), Mg# from 0.63 to 0.73 (with average of 0.68) and Fe^{3+}# from 0.02 to 0.09 (with average of 0.06).

Ferritchromites have Cr# average values of 0.88, average Mg# of 0.40 and an average Fe^{3+}# of 0.25. MgO is strongly depleted as well as Al_2O_3, whose average content is as low as 4.66 wt%.

5.2. BMM

Awaruite, other Ni-Fe alloys and heazlewoodite are the most abundant phases among BMM. Awaruite has variable Ni and Fe contents, with the former ranging between 70.20 and 79.57 wt% and the latter between 20.55 and 25.51 wt%. One awaruite has 4.06 wt% residual S content. Some Ni-Fe alloys show too high Ni contents to be classified as awaruites. Their Ni content ranges between 81.42 and 83.48 wt%. One Ni-rich alloy contains 7.58 wt% Ir, 3.85 wt% Cu, 2.18 wt% Ru, 1.70 wt% Rh, 0.77 wt% Os, 0.42 wt% As and 0.19 wt% Pt. Awaruites contain up to 1.03 wt% Cu while Cu content of Ni-Fe alloys is higher, up to 3.85 wt% and never below 3 wt%. Awaruites can contain up to 0.10 wt% Os, 0.57 wt% Ir, 0.36 wt% Pt and 0.26 wt% Pd. Ni-Fe alloys show lower PGE contents, with only Ir up to 0.18 wt%.

Heazlewoodite Ni content ranges between 70.81 and 75.81 wt%, with S ranging between 26.50 and 28.69 wt%. Some residual Fe is always present in heazlewoodite, reaching up to 3.25 wt%. PGE content is low but quite different from that of alloys. The highest PGE contents were found for Pt, Ir, Os and Rh, with peak values respectively at 0.86, 0.76, 0.30 and 0.11 wt%.

The few pentlandite grains detected show incipient alteration at different degrees of Ni-enrichment. Ni ranges between 37.81 and 44.01 wt%. Rh, is the most abundant PGE in pentlandite, up to 0.29 wt% followed by Ir, up to 0.16 wt%.

Maucherite is the only As phase detected. Its Ni and As contents range respectively between 51.33 and 53.82 wt% and 45.67 and 49.09 wt%. Maucherites are systematically enriched in Pt, up to 0.71 wt%. Other PGE contents are low with the exception of one grain with 0.45 wt% Ir. One grain is strongly altered into Ni alloy, with just 14.31 wt% As remaining.

Millerite composition ranges between 64.46 and 68.97 wt% for Ni and between 32.73 and 36.32 wt% for S. it can contain up to 0.95 wt% Cu and 0.12 wt% As. PGE content is low, with the exceptions of Pt, up to 0.45 wt% and Ir, up to 0.26 wt%.

Elemental atomic maps (Fig. 6) were acquired on a heazlewoodite grain partially altered into millerite (Fig. 3D). Heazlewoodite substitution by millerite occurs starting from the fractures, from where it extends into the heazlewoodite crystal. Millerite is depleted in Ni, Cu and Pd compared to heazlewoodite, while Rh and Ir contents are about the same in the two phases.

5.3. PGM

The overall compositional range of laurite-erlichmanite is very wide, spanning from 0.17 to 0.97 Ru# (Ru/(Os+Ru) atomic proportion). It ranges from 0.51 to 9.73 wt% and As from 1.33 to 3.45 wt%. Primary euhedral laurites are Ru-rich and show a restricted range of Ru# (0.78-0.94). Laurite-erlichmanite in ployphasic grains, associated to other PGM (mainly PGE alloys) or BMM are often zoned and display a much wider compositional variability.

PGE alloys are mostly found in polyphase aggregates and show variable relationships with laurite-erlichmanite and BMM. They are mainly Os-Ir-Ru alloys, with very variable proportions among these three PGE. Rh contents are low, up to 1.70 wt%, while Pt and Pd are virtually absent. Base metals content in these alloys is very low, less than 1 wt% and is limited to Ni, Fe and minor Cu. Only one PGE sulfide not belonging to the laurite-erlichmanite series was detected. Its composition is that of a cuproiridsite where Ir is partially replaced by Rh and Cu is partially replaced by Fe.

Pt and Pd are very rare in PGM. The former was found only in an Ir-Fe alloy, probably a chengdeite, which contains 4.10 wt% Pt, the latter is present in laurites, but never exceeds 0.40 wt%.

Elemental atomic maps were acquired on the laurite partially replaced by Os-Ir alloy of Fig. 7. In spite of the relatively low quality of the maps, due to the very tiny size of the grain some patterns can be identified. Os, Ir and Cu are enriched in the PGE alloy at the rim, while Ru is enriched in the reaction zone (Fig. 7).

6. Whole rock PGE content

Whole rock PGE content was analyzed for 8 chromitite samples. Chromitite texture, sample location and PGE contents are reported in Table 4.

Total PGE content ranges between 16.6 and 420.9 ppb. Massive chromitites show a much higher average PGE content (163.62 ppb) than banded ones (43.53 ppb), with the only nodular chromitite analysis in an intermediate situation (109.1 ppb).

All samples are enriched in Os and Ru, one of which is invariably the most abundant PGE. The IPGE/PPGE ratio is high, between 4.81 and 19.86, with the exception of the nodular sample from Soghan, with a ratio of 2.14.

7. Discussion

7.1. BMM and PGM primary magmatic assemblage

Primary BMM found in chromitites are usually Ni-Fe sulfides, namely pentlandite and pyrrhotite, stable at T above 550 °C, below which, according to the metal/sulfur ratio, the assemblage breaks up forming millerite, heazlewoodite or awaruite (Kullerud, 1963). If some copper is present in the system, also primary minerals in the Ni-Fe-Cu system can be found, such as chalcopyrite or bornite (Proenza et al., 2001). Within Abdasht and Soghan chromitites the only primary BMM found are few pentlandite grains always surrounded by awaruite, and one bornite. They are hosted in the silicate gangue and crystallized after PGM and chromite.

Primary PGM are more easily preserved as they are hosted within chromite. This can explain why they are much more abundant than primary BMM. They are mainly laurites with variable Os content. Laurites are the most abundant primary PGM found within ophiolite chromitites (González-Jiménez et al., 2014 and references therein), and they directly crystallize from the melt (Augè, 1985; Legendre, 1982, Stockman and

Hlava 1984). Stoichiometric laurite can precipitate in equilibrium with Os-Ir alloys at 1200 – 1300 °C and logfS_2 between -1.2 and -2 (Andrews and Brenan, 2002; Bockrath, 2004; Brenan and Andrews, 2001). Os becomes more soluble in laurite with decreasing temperature and/or increasing fS_2, producing minerals with compositions within the laurite-erlichmanite endmembers (Brenan and Andrews, 2001). The variability of Os and Ru content of Abdasht and Soghan laurites can be related to slightly different degrees of evolution of the melt, with Ru content decreasing with cooling and/or increasing of fS_2.

7.2. Desulfurization

The alteration of pentlandite into heazlewoodite and finally awaruite and the occurrence of millerite, godlevskite and native metals are common features in serpentinized dunites and chromitites (Frost, 1985; Melcher et al., 1997; Prichard et al., 1994; Tzamos et al., 2016), and they can be linked to a desulfurization event. Low fO_2 and low fS_2 fluids can be related to serpentinization (Chamberlain et al., 1966; Kanehira 1975). Desulfurization can occur in different stages. Below 550 °C pentlandite is replaced by heazlewoodite (Kullerud, 1963) while the formation of alloys has been estimated at 360-445 °C (Tzamos et al., 2016). At Abdasht and Soghan secondary sulfides and Ni-Fe alloys make up the majority of the BMM found. The most common BMM are heazlewoodite, awaruite and Ni-rich alloys, all of them found in the silicate matrix, at the rim of chromite grains or associated to fracture zones. Textural evidences show that primary pentlandites were transformed into secondary heazlewoodites and awaruites (Fig. 3 A, B).

The desulfurization within Abdasht-Soghan complex could have therefore followed two possible patterns: a one-step transformation into awaruites, or a two-step alteration: first into heazlewoodites and then into Ni-rich alloys (Fig. 8).

The PGM assemblage (Fig. 9) is also characterized by the presence of alteration phases, especially close to fractures or in contact with the silicate matrix. While Os-Ir alloys are sometimes ascribed to a magmatic environment (Brenan and Andrews, 2001), they can also be the product of alteration of primary laurites due to pervasive percolation of low fS_2 fluids, during metamorphic events (Garuti and Zaccarini, 1997; González-Jiménez et al., 2014; Prichard et al., 2008; Proenza et al., 2007; Zaccarini et al., 2005). Textural evidence argues for a secondary formation of the PGE alloys found in Abdasht and Soghan. They are almost invariably found as reaction rim zones of primary laurites, where contacts between laurite and alloy is not

sharp but irregular, in contrast with the euhedral shape of the primary laurite grain (Fig. 5c). Very seldom PGE alloys are not related to laurite. They can be part of a PGM-BMM aggregate (Fig. 4c) or be isolated alloy grains within chromite. In the first case the association with partially or completely desulfurized BMM witnesses the strong alteration of the aggregate and hence argues for an origin of the PGE alloys as completely desulfurized laurites. Only the origin of isolated PGE alloy grains can be doubtful: they could be either primary PGE alloys in equilibrium with a low fS_2 melt or again laurites completely desulfurized during percolation of low fS_2 fluids. The high Os content of the only grain large enough to be analyzed, together with the ubiquitous textural position, associated to pores or fractures within chromites, anyway, strongly argues for their origin as completely altered laurites.

Some PGM grains show intermediate alteration stages where primary laurite rims are S depleted and Os enriched. The best preserved evidence is a polyphasic grain constituted by a laurite core, an Os-poor laurite reaction zone and an Os-rich alloy rim (Fig. 5B).

The composition of secondary BMM and PGM and the general tendency to lose sulfur changing primary sulfide into alloys seem to be the result of a desulfurization event, occurred in a highly reduced environment (Frost, 1985). Such conditions can be achieved during the early stages of serpentinization, (Garuti and Zaccarini, 1997; González-Jiménez et al., 2011, Prichard et al., 1994), that affected not only primary sulfides (e.g. pentlandites), but also the PGM reached by the fluids. The possibility that desulfurization and PGE remobilization were caused by ferrian chromitization fluids was ruled out because of the presence of altered PGM even in samples which completely lack ferrian-chromitization.

7.3. PGE mobility during desulfurization

Several Authors describe post-magmatic PGE remobilization (e.g. Proenza et al., 2007; Tsoupas and Economou-Eliopoulos, 2008; Uysal et al., 2009; Zaccarini et al., 2005, 2008, 2009), fewer works relate it to serpentinization. Prichard et al. (1994) suggest that Pt- and Pd-bearing alloys in chromitites from Shetland ophiolite derived from alteration of magmatic PGM during serpentinization with a mobility of PGE of just few microns. Garuti and Zaccarini (1997) argued that a secondary awaruite-PGE alloys assemblage in Vourinos chromitite was due to desulfurization of the primary BMM-PGM assemblage during serpentinization. González-Jiménez et al. (2010) ascribe the formation of a secondary BMM-PGM

assemblage along fractures and cracks of chromite grains in the Dobromirtsi chromitites to the percolation of altering fluids, with a combination of reducing and oxidizing events, related to regional metamorphism. Textural evidence suggests a partial and selective mobility of PGE during serpentinization of Abdasht and Soghan chromitites. Serpentinizing low-fS_2 fluids reacted with primary laurites to form PGE alloys whose composition is determined by the differential behavior of PGE. Mineralogy and texture of alloy-laurite composite grains suggests that PGE alloy is the phase in equilibrium with serpentinizing fluids and that the reaction progresses from the rim towards the core.

A differential mobility of PGE during post-magmatic processes was observed in chromitites, mainly through textural evidences and comparison between primary and secondary PGM compositions. Variable laurite compositions and laurite grain zonings are ambiguous clues as magmatic and postmagmatic signatures can be superimposed, so they can be better interpreted when associated to secondary PGE alloys. Zaccarini et al. (2005) studied PGE mobility in eclogite facies metamorphosed chromitite-bearing serpentinites. Here Os-rich magmatic laurites are partially altered into Ru-rich laurites, often associated to secondary Os-rich alloy. This evidence argues for a mobilization of Os and minor Ir during maetamorphism at relatively high temperatures and decreasing fS_2. Low fS_2 and formation of Os-rich or Ru-rich alloys is a common feature of secondary PGM assemblages (Proenza et al., 2007; Uysal et al., 2009; Zaccarini et al., 2005, 2008, 2009). This implies a mobility of PGE (at least of Os, Ir and Ru) at the micrometric scale due to subsolidus diffusion as, with lowering fS_2, alloys became the stable PGE phases. In these conditions Os appears more mobile than Ru as Os-alloys are the most widespread feature (Zaccarini et al., 2005). In Abdasht-Soghan chromitites, too, textural evidence argues for a local (micrometric) remobilization where Os is the most mobile PGE, thus forming Os-rich alloy, while Ru is retained in laurite, resulting in the Ru-rich laurite of the reaction zone of Fig. 5B.

The subsolidus diffusion of PGE in order to attain the mineralogical assemblage stable at the new conditions, mainly a low fS_2, could also be accompanied by larger scale mobility of PGE due to their solubility in the desulfurizing fluids. This possibility is supported by the evidence that Os-rich alloy grains, derived from complete alteration of primary laurites, have PGE contents different from those of laurite itself. We exploited the opportunity offered by a partially altered laurite grain (Fig. 5B), where a primary laurite core is preserved, together with secondary Os-rich alloy and Ru-rich laurite reaction zone, in order to calculate a

PGE mass balance. This offers an insight on long range PGE mobility, due to solubility in desulfurizing fluids that pervasively percolated the rock assemblage during serpentinization.

7.3.1 *Desulfurization reaction mass balance*

The most favourable condition showing the progressive changes in mineralogy and composition of BMM and PGM and allowing to infer PGE re-mobilization during fluid percolation in subsolidus is provided by the occurrence of polyphasic PGM grains. A polyphasic grain with a laurite core surrounded by a PGE alloy rim (Fig. 5B) provides an insight on the desulfurization process that affected all the samples. The two phases are not in equilibrium as witnessed by the presence of a thin reaction zone systematically interposed between laurite and alloy. The whole PGM assemblage is a former primary euhedral laurite grain that underwent a partial desulfurization due to the percolation of a desulfurizing fluid along grain boundary. The former rims are enough preserved to show the euhedral shape of the primary laurite but anyway each grain side is not straight but shows minor irregularities and embayments, suggesting that the present assemblage occupies a volume smaller than the primary one, in agreement with a mass loss from the grain due to loss of sulfur and PGE.

Primary laurite and secondary alloy show very different compositions. The former has a composition that well fits the one of all primary laurites detected, Ru-rich and low in Ir. The latter is depleted in Ru and enriched both in Os and Ir. Rh is a minor constituent of both phases and is depleted in the alloy. Pt and Pd are always too low to show meaningful trends. Finally, alloy shows a depletion in As and an enrichment in Cu compared to laurite.

The mass balance is aimed to quantify the amount of each element lost or gained at the intermediate and final stages of desulfurization. The desulfurization parameter used is the S content of the whole assemblage and the elements considered are Os, Ir, Ru and Rh, among PGE, to which Cu and As were added, as all these elements show high enough contents in the PGM phases to provide reliable results.

For the mass balance calculation, we assume, accordingly to the mineralogical and textural evidence, that laurite is the primary PGM, predating host chromite formation, and its composition is in equilibrium with the melt from which it crystallized. The alloy is assumed to be the phase in equilibrium with the desulfurizing

fluids that pervasively permeated the rock. The present multiphasic assemblage is a transitory stage that was frozen at some point during the ongoing desulfurization process and provides information on the elements flow, in or out of the PGM at an intermediate stage of desulfurization.

Calculations of element losses and gains are based on the measurement of areas occupied by the different phases (Table 5). The problem of transforming 2D areal data into 3D volume data has been long debated (e.g. Shumaker, 1990), and finds several applications in the reconstruction of crystal sizes and crystal size distribution (e.g. Berger et al., 2011 and references therein; Jerram et al., 2009). The availability of only one randomly oriented section of the object anyway does not preclude the possibility to get a reliable estimate of the volumes occupied by the three phases. Textural data allow to identify a simple model that can reliably provide 3D information on the relative volumes of the phases involved. Due to the concentric disposal of the three phases and the roughly equidimensional shape of primary euhedral laurite the simple model chosen is that of three concentric spheres. The inner sphere has a radius equivalent to that of a circle having the area of the primary laurite. The intermediate and outer sphere volumes were calculated adding the areas of the reaction zone and alloy respectively. The volume occupied by the primary laurite corresponds to that of the inner sphere and the volumes occupied by the reaction zone and alloy are calculated as differences respectively between the intermediate and inner sphere and between the outer and intermediate sphere.

Finally, the total area was normalized to 100. With such assumptions volume of phase i is calculated as:

$V_n = 4/3\ \pi^{-0.5}\ ((\sum A_n)^{1.5} - (\sum A_{n-1})^{1.5})$

where A_n is the measured area of phase n, $A_0 = 0$ as primary laurite is modeled as the innermost sphere and n = 1, 2, 3 respectively for primary laurite, reaction zone and alloy.

Mass of the phases was then calculated assuming the most reliable density value for each phase

$m_n = d_n * V_n$

where d_n is the density of phase n. For laurite-erlichmanite solid solution a weighted average density between the two end members was used, for alloy a weighted average between the pure metals.

The initial mass of primary laurite is unknown. As we do not know what would be the size of final alloy after complete desulfurization we cannot calculate an absolute value for the amount of each element gained or lost except for sulfur that is completely lost, but it is still possible to calculate the balance of the elements relative to each other. We then chose as reference element Os to which mass balances of other elements are

calculated. This choice is based on the fact that Os is the least mobile of all PGE and in our samples it is only enriched in the residual phases. We then calculated the mass balance for each element normalized to immobile Os.

In order to normalize to costant Os we calculated the initial mass of primary laurite as the mass that contains the whole amount of Os.

$m_0 = 100 * m_{Os} / C_{Os,lau}$

where m_{Os} is calculated as $\sum n [(m_n * C_{Os,n}/100)]$

The initial mass of each element is then calculated as:

$m_{i0} = (C_{i,lau} * m_0)/100$

where $C_{i,lau}$ is the concentration of element i in primary laurite.

The current mass, the mass after partial desulfurization, of each element is:

$m_i = \sum n \; [\![m_n * C_{i,n}/100]\!]$

where m_i is the mass of element i, and $C_{i,n}$ is the concentration of element i in phase n in wt%.

In order to calculate the final mass of each element we firstly calculate the final mass of alloy that is necessary to preserve the Os content. This is.

$m_f = 100 * m_{Os} / C_{Os,alloy}$

Then the final mass of each element is:

$m_{if} = (m_f * C_{i,alloy})/100$

where m_{if} is the final mass of element i and $C_{i,alloy}$ is the concentration of the element i in the alloy.

Finally, the loss or gain of each element is calculated as the difference between its final and initial mass normalized to initial mass and expressed as %. Mass variation after partial desulfurization will be:

$\Delta m_{ip} = 100*(m_i - m_{i0})/ m_{i0}$

And mass variation after complete desulfurization will be:

$\Delta mi = 100*(m_{if} - mi_0)/ mi_0$

All parameters are reported in Table 5 and Δm_i as a function of sulfur loss is reported in Table 6 and Fig. 10 for all elements except copper that has a too high gain to be shown in figure. Data show a correlation between the parameters that is clearly not linear and hence the mobility trend is shown in figure through a parabolic curve.

Two elements, Cu and Ir, show a positive Os normalized trend and are added to the system during interaction with fluids. Cu content is very low in the primary laurite and its relatively high content in the alloy is almost completely due to addition from fluids. Cu input during percolation of fluids has been already observed in ultramafic rocks, mainly as native copper within later dykes (Eslami et al., 2018), suggesting that copper is brought into the system by low fS_2 fluids. Such evidence was also found in an Abdasht sample where native copper was detected. Iridium is the only PGE showing a mass increase during the sulfurization, up to 18.6 %. This Iridium input in the alloy can be due to low partition coefficient between fluid and alloy accompanied by a relatively high concentration in the fluid. Such high concentration could be explained by release of Ir from olivine during serpentinization that increases concentration in fluid.

Most of the PGE loss is due to release of Ru from primary laurite. Its final content is reduced to about one fifth of the initial one. The mobility of Ru suggests that this element has a partition coefficient between fluid and alloy much higher than both Ir and Os and can be easily released to the fluids. On the other hand, the high Ru content of the reaction zone, higher than that of both reacting phases, suggests that Ru diffusivity is low. The reaction zone releases Os but not Ru to the alloy and hence inducing the Ru high content of the reaction zone. The low subsolidus diffusivity of Ru could also explain the convex shape of the Ru release curve, as sulfur is remobilized earlier than Ru. Rh is the most mobile PGE. Its content decreases quickly with desulfurization, tracing a concave desulfurization curve. This suggests that Rh diffusivity and its fluid to alloy partition coefficient are both high. In spite of its fast release Rh mobility effect on total mass balance is very limited due to low Rh content of primary laurite. Finally, As, as expected, shows a mobility similar to that of sulfur, with the low curvature of the desulfurization trend that could be indicative of a linear correlation between the depletion of these two elements.

7.3.2 *PGE patterns*

PGE contents in Abdasht-Soghan chromitites range from 17 ppb in banded chromitites to 421 ppb in massive chromitites and increase with abundance of chromite in the rock. This can be explained with the capacity of chromite to entrap primary PGM during early stages of crystallization. Mantle normalized PGE patterns (Fig. 11) are similar between the two massifs and are characterized by a general negative slope from IPGE to PPGE, with a marked drop between Rh and Pt. The low Pt and Pd contents depicted by the sharp drop in the pattern between Rh and Pt is a common feature of ophiolite chromitites (e.g. Economou-Eliopoulos, 1996;

Grieco et al., 2004; Proenza et al., 2007; Uysal et al., 2009; Zhou et al., 1998). Such sharp drop pattern was also previously found in other chromitites from Southern Iran (Jannessary et al., 2012; Najafzadeh et al., 2014) and in the Abdasht massif (Jannessary et al., 2012). Within this general framework Abdasht and Soghan patterns show some peculiaritites. While usually IPGE trend in mantle patterns shows a peak for Ru (Fig. 11), our samples show two peaks, corresponding to Os and Ru, with Os mantle normalized content that is often higher than Ru one. Another peculiarity is the presence of two patterns from banded chromitites with relatively low chromite content and much lower PGE content (less than 30 ppb) that are relatively flattened, with much less marked drop after Rh and no Ru peak. The PGE patterns suggest a loss of Ru compared to Ir and Os that produces a double peak pattern or, in the most altered samples, a flat pattern with lower total PGE content. This kind of feature in whole rock PGE patterns is not observed in all desulfurized chromitites. The patterns in chromitites studied by Proenza et al. (2007), Tsoupas and Economou-Eliopoulos (2008) and Zaccarini et al. (2008) do not show such kind of trends. This can be either due to absence of PGE mobility in the fluids in the samples they studied or to short range mobility, with incorporation of PGE in secondary phases. This latter process could also have been occurred in Abdasht and Soghan chromitites as some secondary BMM show enrichment in some PGE, mostly Pt and Pd. On the other hand, some PGE patterns enriched in Os are shown by Uysal et al. (2009) in chromitites from Mugla, Turkey, also hosting altered PGM assemblages. Also, Grieco et al. (2007) report double peak patterns in chromitites with altered PGM assemblages from Nurali ophiolite. Here the most widespread features of PGM are an irregular core to rim zoning of laurite, where rims are systematically Os-rich, and the abundance of Os-rich alloys.

In order to check if the two peculiar features, Os peak and low total PGE flat patterns, can be related to the desulfurization process we compared the relative abundance of Os, Ru and Ir in the whole rock with the effect of desulfurization on PGM composition (Fig. 12). The desulfurization curves of Os, Ir and Ru (Fig. 10) were used to plot a desulfurization trend in the Os-Ru-Ir diagram. This can be compared to the relative abundance of Ru, Os and Ir in whole rock. The full set of samples from Abdasht and Soghan, comprising those from Jannessary et al. (2012) plot close to the desulfurization line, showing that desulfurization of laurite is the main postmagmatic process that affected PGM. Samples from Jannessary et al. (2012) were probably collected from a less serpentinized part of the ore, as also suggested by their host rock analysis of a dunite. They show a desulfurization degree between 0 and 75%, that, due to the downward convexity of the

Ru remobilization curve (Fig. 10) results in a little change of the IPGE relative ratios and hence in PGE normalized patterns similar to those of average ophiolite chromitites, showing a single Ru peak.

Our samples were collected from strongly serpentinized portions of the ore and were affected by 75 to 100% desulfurization. In these conditions most of the Ru is remobilized, causing a relative increase of Os that results in the double peak pattern. Within this framework the two samples with low PGE contents and flat patterns are those with the highest degree of desulfurization. We can argue that in these conditions all PGE can be remobilized, even though still in the order: Ru>>Os>Ir. Grieco et al. (2004) observed similar changes of PGE contents and chondritic patterns shapes in Finero chromitites. The patterns change from negative to positive slopes in IPGE portion with decreasing total PGE content. They ascribed this effect to the percolation of metasomatizing fluids that were responsible for the re-hydration of harzburgite due to crystallization of secondary amphibole. These fluids selectively leached PGE giving, as a result, the inversion of slope in the IPGE portion of the patterns.

It is not possible, due to their low content, to provide reliable information on the behavior of PPGE. According to mass balance Rh is very mobile and this is reflected in its lower content in the most desulfurized samples. PGE whole rock data suggest that Pt and Pd are not depleted in desulfurized samples and a possible clue of this behavior is the presence of an Ir alloy (chengdeite) with 4.10 wt% Pt.

7.4. Late re-sulfurization

The desulfurization process is the main event responsible of the PGE mobility in the two complexes, as suggested by the textural and chemical clues described above. However, there is also evidence of a later resulfurization event, not as pervasive as the desulfurization one and possibly related to circulation of more oxidizing fluids.

The major clue supporting this hypothesis is the partial replacement of heazlewoodite and maucherite by millerite in some sulfide grains (Fig. 6). The event only affected BMM and possibly chromite, while PGM do not seem to have registered this late event.

The late oxidizing event can be correlated to the partial and unevenly distributed chloritization and ferritchomititzation of chromitites. Chromites in Abdasht and Soghan display similar features, plotting within the

same compositional fields (Fig. 13). Ferrian-chromitization is present in both complexes, but it affects small portions of the chromite grains, and follows a common trend from chromite to ferrian-chromite (Fig. 13).

Alteration of chromite into ferrian chromite is a well-known feature within ophiolite complexes, and the formation of this secondary phase has been attributed to a number of conditions, occurring mainly during metamorphism or hydrothermal events. Merlini et al. (2009) report the formation of ferrian chromite and chlorite through an oxidation reaction between chromite and serpentine. Proenza et al. (2004) and Mellini et al. (2005) suggest the formation of ferrian chromite and chlorite during low-P low-T retrograde metamorphism, at hydrous, oxidizing conditions. Mukherjee (2010) reports formation of ferrian chromite during low-T hydrothermal events.

Ferrian chromite is not systematically present neither in the two complexes nor from sample to sample. This could suggest that the formation of ferrian chromite rims is not coeval with the massive serpentinization event responsible for the alteration of BMM and PGM into alloys, but it is due to a later event, maybe the same that caused minor and partial resulfurization, less pervasive than the previous one. The presence of Cr-chlorite sometimes associated to ferrian chromite rims, is in agreement with a low-T, low-P event, probably at oxidizing conditions, that occurred in a late stage of the alteration history of the massifs and did not affect the PGM assemblage and the PGE whole rock content.

8. Conclusions

Most studies on PGE distribution and mineralogy in ophiolite chromitites deal with the primary magmatic processes that rule their release from the mantle and concentration during chromitite formation. They confirm that the most widespread PGM assemblage in unaltered chromitites is dominated by laurite of different compositions, depending on the different conditions at which crystallization occurs. Even if PGE alloys can be primary phases they are mostly the result of post-magmatic desulfurization. Several studies have shown that PGM can be altered and PGE remobilized during post magmatic processes, related to pervasive percolation of fluids during metamorphic events affecting the rock assemblage. Remobilization occurs mainly at the micrometric scale, where Os usually behaves as the most mobile PGM as it early diffuses in subsolidus from laurite to form Os-rich alloys.

Abdasht and Soghan chromitites underwent an unevenly distributed serpentinization that modified both BMM and PGM assemblages, due to pervasive percolation of low fS_2 fluids. The desulfurization event changed the primary BMM assemblage in a secondary one dominated by Ni-Fe alloy and heazlewoodite. The primary PGM assemblage, dominated by laurite, was also changed into a secondary one dominated by Os-rich PGE and PGE-BM alloys. PGM alteration was less pronounced and more patchy than BMM one due to the preservation of laurites that, being included within chromites, in absence of fractures or cracks, were not reached by the fluids.

PGE remobilization occurred at two different scales. Instability of laurite at low fS_2 resulted in subsolidus diffusion of PGE. Os was the most mobile and the first one to exit laurite lattice to form Os-rich alloys. Mass balance on partially altered laurite, on the other hand, shows that the PGM assemblage lost mainly Ru. A second larger range remobilization hence can be inferred, where Ru acted as the most soluble PGE in the desulfurizing fluids, that differentially remobilized PGE. The mobility of PGE into the fluids follows the order: Ru>>Os>Ir. Less reliable data, due to the lower contents of PPGE, suggest that Rh is more mobile than Ru and that Pt and possibly Pd can be added to some extent to the system by fluids. This larger range mobility affects PGE whole rock content, giving rise to double peak and flat PGE patterns.

Results show that differential mobility of PGE during the percolation of low fS_2 metamorphic fluids, can strongly affect PGE distribution and mineralogy within ophiolite chromitites and can play an important role in the economic assessment of this kind of PGE ore. Further studies, devoted to constrain the extent of PGE mobility and the fate of PGE remobilized by fluids could also be useful in the economic evaluation of PGE.

Acknowledgements

We wish to acknowledge the Italian Ministry of Education (MIUR) that partially supported this work through the project "Dipartimenti di Eccellenza 2017". We also acknowledge the reviewers who helped us improve the original manuscript with their valuable comments.

References

Ahmadipour, H., 2000. Petrology and geochemistry of Soghan and Abdasht ultramafic-mafic complexes, north-west of Dowlatabad Baft. Unpublished Ph. D. dissertation, Tarbiat Modares University (in Persian).

Ahmadipour, H., Sabzehei, M., Emami, M., Whitechurch, H., Rastad, E., 2003. Soghan complex as an evidence for paleospreading center and mantle diapirism in Sanandaj-Sirjan zone (south-east Iran).

Ahmed, A.H., 2007. Diversity of platinum-group minerals in podiform chromitites of the late Proterozoic ophiolite, Eastern Desert, Egypt: genetic implications. Ore Geology Reviews, 32(1-2), 1-19.

Andrews, D.R., Brenan, J.M., 2002. Phase-equilibrium constraints on the magmatic origin of laurite+ Ru–Os–Ir alloy. The Canadian Mineralogist, 40(6), 1705-1716.

Auge, T., 1985. Platinum-group-mineral inclusions in ophiolitic chromitite from the Vourinos Complex, Greece. The Canadian Mineralogist, 23(2), 163-171.

Ballhaus, C., Ryan, C.G., 1995. Platinum-group elements in the Merensky reef. I. PGE in solid solution in base metal sulfides and the down-temperature equilibration history of Merensky ores. Contributions to Mineralogy and Petrology, 122(3), 241-251.

Berger A., Herwegh M., Schwarz J.O., Putlitz B., 2011. Quantitative analysis of crystal/grain sizes and their distributions in 2D and 3D. J. Struct. Geol., 33, 12, 1751-1763. doi:10.1016/j.jsg.2011.07.002

Bockrath C., Ballhaus C., Holzheid A., 2004. Fractionation of the platinum-group elements during mantle melting. Science, 305(5692), 1951-1953.

Brenker, F.E., Meibom, A., Frei, R., 2003. On the formation of peridotite-derived Os-rich PGE alloys. American Mineralogist, 88(11-12), 1731-1740.

Brenan, J.M., Andrews, D., 2001. High-temperature stability of laurite and Ru–Os–Ir alloy and their role in PGE fractionation in mafic magmas. The Canadian Mineralogist, 39(2), 341-360.

Chamberlain, J.A., 1966. Heazlewoodite and awaruite in serpentinites of the Eastern Townships, Quebec. The Canadian Mineralogist, 8(4), 519-522.

Dai, J.G., Wang, C.S., Hébert, R., Santosh, M., Li, Y.L., Xu, J.Y. 2011. Petrology and geochemistry of peridotites in the Zhongba ophiolite, Yarlung Zangbo Suture Zone: implications for the Early Cretaceous intra-oceanic subduction zone within the Neo-Tethys. Chemical Geology, 288(3-4), 133-148.

Economou, M.I., 1986. Platinum-group elements (PGE) in chromite and sulfide ores within the ultramafic zone of some Greek ophiolite complexes. Metallogeny of basic and ultrabasic rocks, 441-453.

Economou-Eliopoulos, M., 1996. Platinum-group element distribution in chromite ores from ophiolite complexes: implications for their exploration. Ore Geology Reviews, 11(6), 363-381.

Eslami, A., Grieco, G., Montanini, A., Cavallo, A., Arai, L.E., Szabo, C., Marchesi, C., 2018. Mineralogy of Cu-rich hydrothermally altered pyroxenites in the Cheshmeh-Bid chromitite deposit, Khajeh-Jamali ophiolitic massifs, Iran: a first report. 3rd European Mantle Workshop, Pavia, 26-28th June 2018, Abstracts, pag. 42

Fleet, M.E., Crocket, J.H., Liu, M., Stone, W.E., 1999. Laboratory partitioning of platinum-group elements (PGE) and gold with application to magmatic sulfide–PGE deposits. Lithos, 47(1-2), 127-142.

Frost, B.R., 1985. On the stability of sulfides, oxides, and native metals in serpentinite. Journal of Petrology, 26(1), 31-63.

Garuti, G., Zaccarini, F., 1997. In situ alteration of platinum-group minerals at low temperature; evidence from serpentinized and weathered chromitite of the Vourinos Complex, Greece. The Canadian Mineralogist, 35(3), 611-626.

Gervilla, F., Proenza, J.A., Frei, R., González-Jiménez, J.M., Garrido, C.J., Melgarejo, J.C., Meibom, A., Díaz-Martínez, R, Lavaut, W., 2005. Distribution of platinum-group elements and Os isotopes in chromite ores from Mayarí-Baracoa Ophiolitic Belt (eastern Cuba). Contributions to Mineralogy and Petrology, 150(6), 589-607.

González-Jiménez, J.M., Gervilla, F., Proenza, J.A., Kerestedjian, T., Augé, T., Bailly, L., 2009. Zoning of laurite (RuS_2)–erlichmanite (OsS_2): implications for the origin of PGM in ophiolite chromitites. European Journal of Mineralogy, 21(2), 419-432.

González- Jiménez, J.M., Gervilla, F., Kerestedjian, T., Proenza, J.A., 2010. Alteration of Platinum- Group and Base- Metal Mineral Assemblages in Ophiolite Chromitites from the Dobromirtsi Massif, Rhodope Mountains (Bulgaria). Resource geology, 60(4), 315-334.

González-Jiménez, J.M., Proenza, J.A., Gervilla, F., Melgarejo, J.C., Blanco-Moreno, J.A., Ruiz-Sánchez, R., Griffin, W.L., 2011. High-Cr and high-Al chromitites from the Sagua de Tánamo district, Mayarí-Cristal ophiolitic massif (eastern Cuba): Constraints on their origin from mineralogy and geochemistry of chromian spinel and platinum-group elements. Lithos, 125(1-2), 101-121.

González-Jiménez, J.M., Griffin, W.L., Gervilla, F., Proenza, J.A., O'Reilly, S.Y., Pearson, N.J., 2014. Chromitites in ophiolites: How, where, when, why? Part I. A review and new ideas on the origin and significance of platinum-group minerals. *Lithos*, *189*, 127-139.

Grieco, G., Ferrario, A., Mathez, E.A., 2004. The effect of metasomatism on the Cr-PGE mineralization in the Finero Complex, Ivrea Zone, Southern Alps. Ore Geology Reviews, 24(3-4), 299-314.

Grieco, G., Diella, V., Chaplygina, N.L., Savelieva, G.N., 2007. Platinum group elements zoning and mineralogy of chromitites from the cumulate sequence of the Nurali massif (Southern Urals, Russia). Ore Geology Reviews, 30(3-4), 257-276.

Jackson, S.E., Fryer, B.J., Gosse, W., Healey, D.C., Longerich, H.P., Strong, D.F., 1990. Determination of the precious metals in geological materials by inductively coupled plasma-mass spectrometry (ICP-MS) with nickel sulphide fire-assay collection and tellurium coprecipitation. Chemical Geology, 83(1-2), 119-132.

Jannessary, M.R., Melcher, F., Lodziak, J., Meisel, T.C., 2012. Review of platinum-group element distribution and mineralogy in chromite ores from southern Iran. Ore Geology Reviews, 48, 278-305.

Jerram, D.A., Mock A., Davis G.R., Field M., Brown R.J., 2009. 3D crystal size distributions: A case study on quantifying olivine populations in kimberlites, Lithos, 112, 1, pp. 223-235.

Kanehira, K., Banno, S., yui, S., 1975. Awaruite, heazlewoodite, and native copper in serpentinized peridotite from the Mineoka district, southern Boso Peninsula. The Journal of the Japanese Association of Mineralogists, Petrologists and Economic Geologists, 70(11), 388-394.

Kullerud, G., 1963. Thermal stability of pentlandite. The Canadian Mineralogist, 7(3), 353-366.

Legendre, O., 1982. Thèse Doctoral 3o Cycle Minèralogie et geèochimie des platinoïdes dans les chromitites ophiolitiques, 6. Université de Paris, p. 171.

Lorand, J.P., Luguet, A., Alard, O., 2008. Platinum-group elements: a new set of key tracers for the Earth's interior. Elements, 4(4), 247-252.

McCall, G.J.H., 1985. Explanatory text of Minab quadrangle map, J 13. Geological Survey of Iran, 530 pp.

McDonough, W.F., Sun, S.S., 1995. The composition of the Earth. Chemical geology, 120(3-4), 223-253.

Melcher, F., Grum, W., Simon, G., Thalhammer, T.V., Stumpfl, E.F., 1997. Petrogenesis of the ophiolitic giant chromite deposits of Kempirsai, Kazakhstan: a study of solid and fluid inclusions in chromite. Journal of Petrology, 38(10), 1419-1458.

Mellini, M., Rumori, C., Viti, C., 2005. Hydrothermally reset magmatic spinels in retrograde serpentinites: formation of "ferritchromit" rims and chlorite aureoles. Contributions to Mineralogy and Petrology, 149(3), 266-275.

Merlini, A., Grieco, G., Diella, V., 2009. Ferritchromite and chromian-chlorite formation in mélange-hosted Kalkan chromitite (Southern Urals, Russia). American Mineralogist, 94(10), 1459-1467.

Mukherjee, R., Mondal, S.K., Rosing, M.T., Frei, R., 2010. Compositional variations in the Mesoarchean chromites of the Nuggihalli schist belt, Western Dharwar Craton (India): potential parental melts and implications for tectonic setting. Contributions to Mineralogy and Petrology, 160(6), 865-885.

Mungall, J.E., Naldrett, A.J., 2008. Ore deposits of the platinum-group elements. Elements, 4(4), 253-258.

Najafzadeh, A.R., Ahmadipour, H., 2014. Using platinum-group elements and Au geochemistry to constrain the genesis of podiform chromitites and associated peridotites from the Soghan mafic–ultramafic complex, Kerman, Southeastern Iran. Ore Geology Reviews, 60, 60-75.

Najafzadeh, A.R., Ahmadipour, H., 2016. Geochemistry of platinum-group elements and mineral composition in chromitites and associated rocks from the Abdasht ultramafic complex, Kerman, Southeastern Iran. Ore Geology Reviews, 75, 220-238.

O'Neill, H.S.C., Dingwell, D.B., Borisov, A., Spettel, B., Palme, H., 1995. Experimental petrochemistry of some highly siderophile elements at high temperatures, and some implications for core formation and the mantle's early history. Chemical Geology, 120(3-4), 255-273.

Prichard, H.M., 1986. Platinum-group minerals in the Shetland ophiolite. Metallogeny of basic and ultrabasic rocks, 395-414.

Prichard, H.M., Ixer, R.A.F., Lord, R.A., Maynard, J.B., Williams, N., 1994. Assemblages of platinum-group minerals and sulfides in silicate lithologies and chromite-rich rocks within the Shetland ophiolite. The Canadian Mineralogist.

Prichard, H.M., Neary, C.R., Fisher, P.C., O'hara, M.J., 2008. PGE-rich podiform chromitites in the Al 'Ays ophiolite complex, Saudi Arabia: an example of critical mantle melting to extract and concentrate PGE. Economic Geology, 103(7), 1507-1529.

Prichard, H.M., Lord, R.A., 1988. The Shetland ophiolite: evidence for a supra-subduction zone origin and implications for platinum-group element mineralization. In Mineral deposits within the European Community (pp. 289-302). Springer, Berlin, Heidelberg.

Proenza, J.A, Gervilla, F., Melgarejo, J., Vera, O., Alfonso, P., Fallick, A., 2001. Genesis of sulfide-rich chromite ores by the interaction between chromitite and pegmatitic olivine–norite dikes in the Potosí Mine (Moa-Baracoa ophiolitic massif, eastern Cuba). Mineralium deposita, 36(7), 658-669.

Proenza, J.A., Ortega-Gutiérrez, F., Camprubí, A., Tritlla, J., Elías-Herrera, M., Reyes-Salas, M., 2004. Paleozoic serpentinite-enclosed chromitites from Tehuitzingo (Acatlán Complex, southern Mexico): a petrological and mineralogical study. Journal of South American Earth Sciences, 16(8), 649-666.

Proenza, J.A., Zaccarini, F., Lewis, J.F., Longo, F., Garuti, G., 2007. Chromian spinel composition and the platinum-group minerals of the PGE-rich Loma Peguera chromitites, Loma Caribe peridotite, Dominican Republic. The Canadian Mineralogist, 45(3), 631-648.

Righter, K., 2003. Metal-silicate partitioning of siderophile elements and core formation in the early Earth. Annual Review of Earth and Planetary Sciences, 31(1), 135-174.

Sabzehei, M., 1974. Les melange ophiolitiques de la region d'Esfandegheh, these d'etate.

Sabzehei, M., 1998. Upper protrozoic-Lower paleozoic ultramafic-mafic association of south-east Iran, Product of an ophiolitic magma of komatiitic affinity. In International Ophiolite Symposium Abstracts, Finland, 1998 (Vol. 201).

Schumaker L.L., 1990. Reconstructing 3D Objects from Cross-Sections. In: Dahmen W., Gasca M., Micchelli C.A. (eds) Computation of Curves and Surfaces. NATO ASI Series (Series C: Mathematical and Physical Sciences), vol 307. Springer, Dordrecht.

Stockman, H.W., Hlava, P.F., 1984. Platinum-group minerals in alpine chromitites from southwestern Oregon. Economic Geology, 79(3), 491-508.

Torres-Ruiz, J., Garuti, G., Gazzotti, M., Gervilla, F., Hach-Ali, P.F., 1996. Platinum-group minerals in chromitites from the Ojen lherzolite massif (Serrania de Ronda, Betic Cordillera, Southern Spain). Mineralogy and Petrology, 56(1-2), 25-50.

Tredoux, M., Lindsay, N.M., Davies, G., McDonald, I., 1995. The fractionation of platinum-group elements in magmatic systems, with the suggestion of a novel causal mechanism. South African Journal of Geology, 98(2), 157-167.

Tsoupas, G., Economou-Eliopoulos, M., 2008. High PGE contents and extremely abundant PGE-minerals hosted in chromitites from the Veria ophiolite complex, northern Greece. Ore Geology Reviews, 33(1), 3-19.

Tzamos, E., Filippidis, A., Michailidis, K., Koroneos, A., Rassios, A., Grieco, G., Pedrotti, M., Stamoulis, K., 2016. Mineral chemistry and formation of awaruite and heazlewoodite in the Xerolivado chrome mine, Vourinos, Greece. Bulletin of the Geological Society of Greece, 50(4), 2047-2056.

Uysal, I., Tarkian, M., Sadiklar, M.B., Zaccarini, F., Meisel, T., Garuti, G., Heidrich, S., 2009. Petrology of Al-and Cr-rich ophiolitic chromitites from the Muğla, SW Turkey: implications from composition of chromite, solid inclusions of platinum-group mineral, silicate, and base-metal mineral, and Os-isotope geochemistry. Contributions to Mineralogy and Petrology, 158(5), 659-674.

Wedepohl, K.H., 1995. The composition of the continental crust. Geochimica et cosmochimica Acta, 59(7), 1217-1232.

Wirth, R., Reid, D., Schreiber, A., 2013. Nanometer-sized platinum-group minerals (PGM) in base metal sulfides: New evidence for an orthomagmatic origin of the Merensky Reef PGE ore deposit, Bushveld Complex, South Africa. The Canadian Mineralogist, 51(1), 143-155.

Zaccarini, F., Proenza, J.A., Ortega-Gutiérrez, F., Garuti, G., 2005. Platinum group minerals in ophiolitic chromitites from Tehuitzingo (Acatlan complex, southern Mexico): implications for post-magmatic modification. Mineralogy and Petrology, 84(3-4), 147-168.

Zaccarini, F., Pushkarev, E., Garuti, G., 2008. Platinum-group element mineralogy and geochemistry of chromitite of the Kluchevskoy ophiolite complex, central Urals (Russia). Ore Geology Reviews, 33(1), 20-30.

Zaccarini, F., Proenza, J.A., Rudashevsky, N.S., Cabri, L.J., Garuti, G., Rudashevsky, V.N., Melgarejo, J.C., Lewis J.F., Longo, F., Bakker R.J., Stanley, C.J., 2009. The Loma Peguera ophiolitic chromitite (Central Dominican Republic): a source of new platinum group minerals (PGM) species. Neues Jahrbuch für Mineralogie-Abhandlungen: Journal of Mineralogy and Geochemistry, 185(3), 335-349.

Zaccarini, F., Singh, A.K., Garuti, G., 2016. Platinum group minerals and silicate inclusions in chromitite from the Naga-Manipur ophiolite complex, Indo-Myanmar orogenic belt, northeast India. The Canadian Mineralogist, 54(2), 409-427.

Zhou, M.F., Sun, M., Keays, R.R., Kerrich, R.W., 1998. Controls on platinum-group elemental distributions of podiform chromitites: a case study of high-Cr and high-Al chromitites from Chinese orogenic belts. Geochimica et Cosmochimica Acta, 62(4), 677-688.

Figure captions

Fig. 1. a. Schematic map of Mesozoic ophiolites in Iran; the studied area is included in the red rectangle; b. simplified geological map of the Abdasht ultramafic complex (modified after Ahmadipour, 2000); c. simplified geological map of the Soghan mafic–ultramafic complex (modified after Ahmadipour et al., 2003).

Fig. 2. BSE image from a deeply Fe-chromititized sample with a late brucite vein. Abbreviations: Cr-chl = Cr-chlorite, Fe-Chr = Fe-chromite, Brc = brucite.

Fig. 3 Back Scattered Electrons (BSE) image (A) and S elemental map (B) of a massive bleb of awaruite with tiny relict inclusions of heazlewoodite from Panjah Metri Mine; BSE image of a bleb of native copper

within Cr-chlorite matrix, close to Fe-chromite (C); BSE image of heazlewoodite grain partially replaced along fractures by millerite (D). Awr: awaruite; Hzl: heazlewoodite; Cu: native copper; Chl: chlorite; Fe-chr: ferrian chromite; Mlr: millerite.

Fig. 4 A) BSE image of primary euhedral laurite inclusion within chromite; B) BSE image of polyphasic inclusion in chromite containing laurite, Cr-chlorite and amphibole, from Omid-Bekhoida Mine, Soghan massif; C) BSE image of polyphasic PGE/BMM aggregate from Abdasht Mine. Two different PGE-base metal alloys are bordered by heazlewoodite on one side and Ni-Cu alloy on the other side. Cr-chl: chromian chlorite; Amp: amphibole; Hzl: heazlewoodite

Fig. 5 A) BSE image of a Os-Ir alloy inclusion in chromite from Panjeh Metri Mine, Soghan massif; B) BSE image of a laurite grain included in chromitite, partially transformed into Os-Ru-Ir alloy and showing a Os-poor laurite reaction rim, Abdasht Mine; C) BSE image of a laurite rimmed by a Os-Ir alloy in chromite from Omid-Bekhoda Mine, Soghan massif. Chr: chromite;

Fig. 6 X-ray elemental distribution maps of the heazlewoodite grain of Fig. 3D, partially replaced by millerite along the crystal fractures.

Fig. 7. X-ray elemental distribution maps of polyphasic aggregate of Fig. 5B.

Fig. 8. –Ternary diagram (at%) of Ni-Fe sulfides and alloys in Abdasht and Soghan, showing the possible desulfurization patterns (red arrows) and the late re-sulfurization process (blue arrow).

Fig. 9. Ternary compositional diagram (at%) of PGM in the Abdasht and Soghan complexes.

Fig. 10. Patterns of Os-normalized PGE losses or gains during desulfurization. On the y-axis are reported losses and gains of Ir, Ru, Rh and As normalized to immobile Os, at three desulfurization steps: 0%, 30% and 100%.

Fig. 11. Mantle-normalized (McDonough and Sun, 1995) PGE patterns of the Abdasht-Soghan complex; yellow field: PGE data of Abdasht and Soghan from Jannessary et al. (2012); grey field: ophiolite chromitites (Proenza et al., 2007)

Fig. 12 Ternary Ru-Os-Ir diagram of PGE concentration in Abdasht and Soghan; blue circles represent different desulfurization stages, from 0% (not desulfurized) to 100% (completely desulfurized); data are from: present work (red squares) and Jannessary et al. (2012) (black squares).

Fig. 13 – XMg vs XCr* diagram of chromites and ferrian chromite samples of the Abdasht-Soghan complex.

Tab. 1 Chromite and Fe-chromite representative analyses; Fe^{3+} recalculated assuming perfect stoichiometry; bdl: below detection limit

Analysis	IRAB-A01	IRSO-A02	IRAB-A01	IRSO-B03	IRSO-B03	IRAB-A03	IRAB-BO3	IRSO-A04	IRAB-BO5	IRAB-B06	IRSO-B01
Texture	massive	massive	massive	dissemin.	dissemin.	dissemin.	banded	banded	banded	nodular	nodular
wt%	Chr	Chr	Fe-Chr	Chr	Chr	Fe-Chr	Chr	Chr	Fe-Chr	Chr	Chr
TiO_2	0.15	0.11	0.15	0.07	0.03	0.10	0.08	0.11	0.14	0.13	0.15
Al_2O_3	10.26	9.70	7.65	19.17	18.52	6.56	11.59	9.99	7.26	13.56	10.55
Cr_2O_3	59.87	60.95	61.90	50.30	50.66	58.46	58.08	60.79	56.53	56.81	60.21
Fe_2O_3	4.20	3.65	3.19	2.05	2.34	6.33	3.83	3.65	9.14	2.01	3.62
FeO	12.18	10.69	16.38	17.94	17.14	22.11	13.26	11.22	16.47	12.82	11.12
MgO	14.47	14.94	11.16	11.44	11.72	7.39	12.63	14.79	11.06	13.87	14.88
NiO	0.11	0.17	0.08	0.01	0.07	bdl	0.14	0.04	0.01	bdl	0.15
Total	100.63	99.85	100.19	100.78	100.24	100.44	100.04	100.27	99.70	99.00	100.33
Atoms											
Ti	0.00	0.00	0.00	0.00	0.00	0.00	0.00	0.00	0.00	0.00	0.00
Al	0.39	0.37	0.30	0.71	0.69	0.26	0.44	0.38	0.28	0.51	0.39
Cr	1.51	1.54	1.62	1.24	1.26	1.57	1.47	1.53	1.48	1.43	1.51
Fe^{3+}	0.10	0.09	0.08	0.05	0.06	0.16	0.09	0.09	0.23	0.05	0.09
Fe^{2+}	0.31	0.29	0.45	0.47	0.45	0.63	0.35	0.30	0.46	0.34	0.30
Mg	0.69	0.71	0.55	0.53	0.55	0.37	0.65	0.70	0.55	0.66	0.70
Ni	0.00	0.00	0.00	0.00	0.00	0.00	0.00	0.00	0.00	0.00	0.00
Mg#	0.69	0.71	0.65	0.53	0.55	0.37	0.65	0.70	0.54	0.66	0.70
Cr#	0.80	0.81	0.84	0.64	0.65	0.86	0.77	0.80	0.84	0.74	0.79
Cr#*	0.76	0.77	0.81	0.62	0.63	0.79	0.74	0.77	0.74	0.72	0.76
Fe^{3+}#	0.08	0.08	0.09	0.04	0.04	0.20	0.08	0.08	0.22	0.04	0.07

Tab 2 – Representative analyses of BMMs of Abdasht and Soghan; Pn: pentlandite, Bn: bornite; Mlr: millerite; Hzl: heazlewoodite; Mcr: maucherite; Awr: awaruite. Bdl: below detection limit

wt%	IRSO-B03 Pn	IRSO-B03 Bn	IRAB-A01 Mlr	IRAB-A01 Mlr	IRAB-A03 Hzl	IRSO-A04 Hzl	IRAB-A01 Mcr	IRAB-B01 Awr	IRSO-A1 Awr	IRAB-B01 Ni-As alloy	IRSO-A2 Ni-Fe alloy
As	0.01	0.07	0.12	0.10	0.03	bdl	48.27	0.14	0.05	14.31	1.98
Os	bdl	0.04	bdl	bdl	bdl	0.13	0.03	0.10	bdl	0.10	bdl
Fe	31.21	11.26	0.30	0.07	0.22	2.32	0.87	23.64	24.22	bdl	10.32
Ir	0.34	bdl	bdl	0.04	0.38	bdl	0.12	bdl	0.57	bdl	0.18
S	34.39	26.57	34.93	35.67	27.33	26.50	bdl	bdl	bdl	1.37	0.02
Ni	34.38	0.18	65.03	65.58	73.86	74.06	[illegible]	75.68	74.55	84.11	83.28
Pt	bdl	bdl	bdl	0.10	bdl	bdl	0.21	0.26	bdl	bdl	0.28
Ru	bdl	0.01	bdl	bdl	bdl	odl	bdl	0.02	0.01	bdl	0.07
Cu	0.37	61.99	0.95	0.16	bdl	bdl	bdl	0.60	bdl	0.04	3.28
Rh	bdl	0.02	0.03	0.03	bdl	bdl	bdl	bdl	bdl	0.06	bdl
Pd	bdl	0.01	bdl	0.01	0.01	bdl	bdl	0.10	0.01	bdl	bdl
Total	100.69	100.16	101.36	101.76	101.82	103.01	100.83	100.53	99.41	100.00	99.41
Atoms											
As	0.00	0.00	0.00	0.00	0.00	0.00	8.00	0.00	0.00	0.13	0.00
Os	0.00	0.00	0.00	0.00	0.00	0.00	0.00	0.00	0.00	0.00	0.00
Fe	4.17	0.97	0.00	0.00	0.01	0.10	0.19	1.00	1.00	0.00	0.96
Ir	0.01	0.00	0.00	0.00	0.00	0.00	0.01	0.00	0.01	0.00	0.00
S	8.00	4.00	1.00	1.00	2.00	2.00	0.00	0.00	0.00	0.03	0.00
Ni	4.37	0.01	1.02	1.00	2.95	3.05	10.86	3.05	2.93	1.00	3.18
Pt	0.00	0.00	0.00	0.00	0.00	0.00	0.01	0.00	0.00	0.00	0.00
Ru	0.00	0.00	0.00	0.00	0.00	0.00	0.00	0.00	0.00	0.00	0.00
Cu	0.04	4.71	0.01	0.00	0.00	0.00	0.00	0.02	0.00	0.00	0.04
Rh	0.00	0.00	0.00	0.00	0.00	0.00	0.00	0.00	0.00	0.00	0.00
Pd	0.00	0.00	0.00	0.00	0.00	0.00	0.00	0.00	0.00	0.00	0.00

Tab 3 – Representative microprobe analyses of PGMs of Abdasht and Soghan. Bdl: below detection limit

wt%	IRSO-A03 Laurite	IRSO-C01 Laurite	IRAB-B05 Laurite	IRAB-B01 Laurite	IRAB-B01 Laurite	IRAB-B05 Cuproiridsite	IRAB-B01 Ru-Os-Ir alloy	IRAB-B01 Ni-Cu-Ir alloy	IRSO-B01 Os-Ir alloy	IRAB-B05 Chengdeite
As	1.46	2.35	2.32	2.04	2.30	0.03	1.00	0.42	0.06	0.02
Os	17.09	8.26	11.53	13.77	3.30	bdl	44.08	0.77	66.25	bdl
Fe	bdl	bdl	bdl	bdl	bdl	3.27	bdl	2.14	0.68	7.28
Ir	9.73	9.19	7.75	6.67	0.51	45.87	25.34	7.58	31.28	87.49
S	33.79	34.38	34.66	35.76	38.74	25.20	bdl	bdl	0.01	bdl
Ni	bdl	bdl	0.05	0.01	0.02	bdl	0.19	81.42	bdl	0.17
Pt	bdl	bdl	bdl	bdl	bdl	bdl	bdl	0.19	bdl	4.10
Ru	36.27	42.64	42.38	40.21	55.14	0.03	26.93	2.18	0.74	bdl
Cu	0.19	0.07	bdl	0.15	0.08	8.78	2.41	3.85	0.07	0.83
Rh	0.43	1.53	1.43	3.38	1.93	13.80	2.24	1.70	0.31	0.07
Pd	0.37	0.48	bdl	0.02	0.21	bdl	bdl	bdl	bdl	0.06
Total	99.33	98.89	100.12	102.01	102.26	97.00	102.19	100.24	99.41	100.00
Atoms										
As	0.04	0.06	0.06	0.05	0.05	0.00	0.05	0.00	0.00	0.00
Os	0.17	0.08	0.11	0.13	0.03	0.00	0.87	0.00	1.00	0.00
Fe	0.00	0.00	0.00	0.00	0.00	0.30	0.00	0.03	0.04	0.29
Ir	0.10	0.09	0.07	0.06	0.00	1.21	0.49	0.03	0.47	1.00
S	2.00	2.00	2.00	2.00	2.00	4.00	0.00	0.00	0.00	0.00
Ni	0.00	0.00	0.00	0.00	0.00	0.00	0.01	1.00	0.00	0.01
Pt	0.00	0.00	0.00	0.00	0.00	0.00	0.00	0.00	0.00	0.05
Ru	0.68	0.79	0.78	0.71	0.90	0.00	1.00	0.02	0.02	0.00
Cu	0.01	0.00	0.00	0.00	0.00	0.70	0.14	0.04	0.00	0.03
Rh	0.01	0.03	0.03	0.06	0.03	0.68	0.08	0.01	0.01	0.00
Pd	0.01	0.01	0.00	0.00	0.00	0.00	0.00	0.00	0.00	0.00

Tab 4 - Whole rock PGE concentration (ppb) in the Abdasht and Soghan complexes.

	Texture	Os	Ir	Ru	Rh	Pt	Pd	Total PGE	IPGE	PPGE	IPGE/PPGE
IRAB-A02	massive	46.50	27.40	77.10	7.00	5.68	2.05	165.73	151.00	14.73	10.25
IRAB-B01	massive	149.00	62.80	177.00	12.30	4.23	15.60	420.93	388.80	32.13	12.10
IRAB-B03	banded	6.91	2.59	4.58	0.63	1.16	0.70	16.57	14.08	2.49	5.65
IRAB-B04	banded	33.90	13.00	38.70	2.16	1.18	0.97	89.91	85.60	4.31	19.86
IRSO-A01	massive	29.00	14.30	42.70	2.48	1.85	2.22	92.55	86.00	6.55	13.13
IRSO-A03	banded	5.81	3.91	6.71	1.07	4.91	1.69	24.10	16.43	7.67	2.14
IRSO-B01	nodular	27.70	15.30	47.30	3.09	6.47	9.21	109.07	90.30	18.77	4.81
IRSO-C02	massive	52.90	26.70	74.20	5.96	2.20	1.66	163.62	153.80	9.82	15.66

Table 5 Parameters used for the calculation and value of input data

A_n laurite	Normalized area of laurite	49.182
A_n reaction zone	Normalized area of reaction zone	43.126
A_n alloy	Normalized area of alloy	7.692
d laurite	density of laurite	7.541
d reaction zone	density of reaction zone	7.082
d alloy	density of alloy	16.809
V_i laurite	Normalized volume of laurite	
V_i reaction zone	Normalized volume of reaction zone	
V_i alloy	Normalized volume of alloy	
m_0	Initial mass of laurite	
m_n	Mass of phase n	
m_{Os}	Mass of Osmium	
$C_{Os,lau}$	Concentration of Os in laurite	
m_{i0}	Initial mass of element i	
$C_{i,lau}$	Concentration of element i in laurite	
m_i	Current mass of each element	
$C_{i,n}$	Concentration of element i in phase n	

m_f	Final mass of alloy	
$C_{Os,alloy}$	Concentration of Os in alloy	
m_{if}	Final mass of element i	
$C_{i,alloy}$	Concentration of element i in alloy	
m_{ip}	Mass of element i after partial desulfurization	
Δm_i	Variation of mass of element i after complete desulfurization	
Δm_{ip}	Variation of mass of element i after partial desulfurization	

Table 6 Results of the mass balance calculations

	Δm_{ip} (wt%)	Δm_i (wt%)
Os	0	0
Ru	-4.93	-79.[illegible]
Ir	5.33	[illegible]8.62
Rh	-37.32	-79.30
Cu	259.73	388.46
As	-18.25	-84.69
S	-29.90	-100

Declaration of interests

☒ The authors declare that they have no known competing financial interests or personal relationships that could have appeared to influence the work reported in this paper.

☐The authors declare the following financial interests/personal relationships which may be considered as potential competing interests:

- Low fS_2 metamorphic fluids partially remobilized PGEs
- Re-mobilization occurred in the order Ru>>Os>Ir
- Mineralogy was also affected with formation of base metal and PGE alloys
- PGE mantle normalized patterns of desulfurized samples show a secondary Os peak

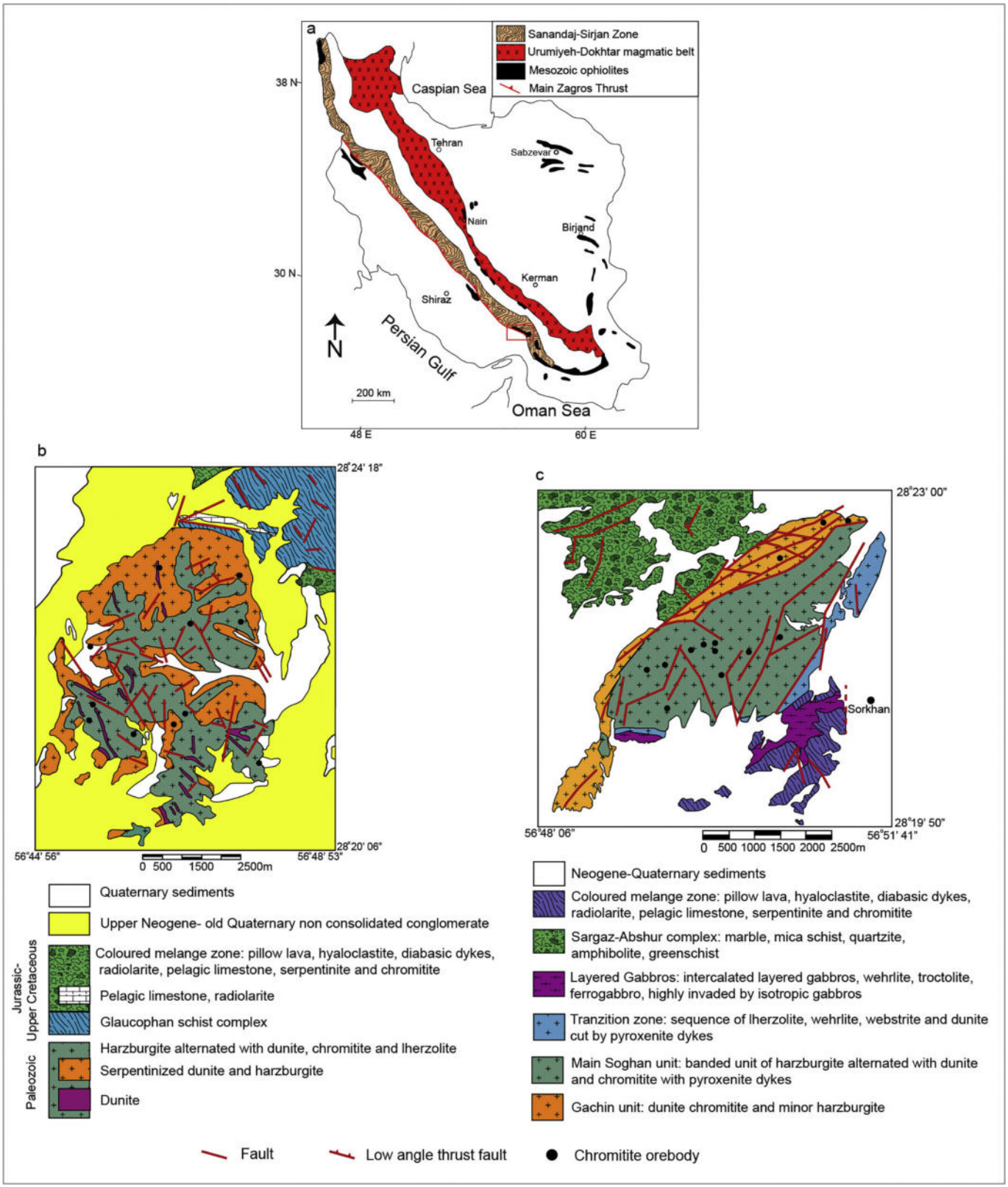
a
Sanandaj-Sirjan Zone
Urumiyeh-Dokhtar magmatic belt
Mesozoic ophiolites
Main Zagros Thrust
Caspian Sea
Tehran
Sabzevar
Nain
Birjand
Kerman
Shiraz
Persian Gulf
Oman Sea
N
200 km
38 N
30 N
48 E
60 E
b
28°24' 18"
28°20' 06"
56°44' 56"
56°48' 53"
0 500 1500 2500m
c
28°23' 00"
28°19' 50"
56°48' 06"
56°51' 41"
Sorkhan
0 500 1000 1500 2000 2500m
Quaternary sediments
Upper Neogene- old Quaternary non consolidated conglomerate
Jurassic-Upper Cretaceous
Coloured melange zone: pillow lava, hyaloclastite, diabasic dykes, radiolarite, pelagic limestone, serpentinite and chromitite
Pelagic limestone, radiolarite
Glaucophan schist complex
Paleozoic
Harzburgite alternated with dunite, chromitite and lherzolite
Serpentinized dunite and harzburgite
Dunite
Neogene-Quaternary sediments
Coloured melange zone: pillow lava, hyaloclastite, diabasic dykes, radiolarite, pelagic limestone, serpentinite and chromitite
Sargaz-Abshur complex: marble, mica schist, quartzite, amphibolite, greenschist
Layered Gabbros: intercalated layered gabbros, wehrlite, troctolite, ferrogabbro, highly invaded by isotropic gabbros
Tranzition zone: sequence of lherzolite, wehrlite, webstrite and dunite cut by pyroxenite dykes
Main Soghan unit: banded unit of harzburgite alternated with dunite and chromitite with pyroxenite dykes
Gachin unit: dunite chromitite and minor harzburgite
Fault
Low angle thrust fault
Chromitite orebody

Figure 1

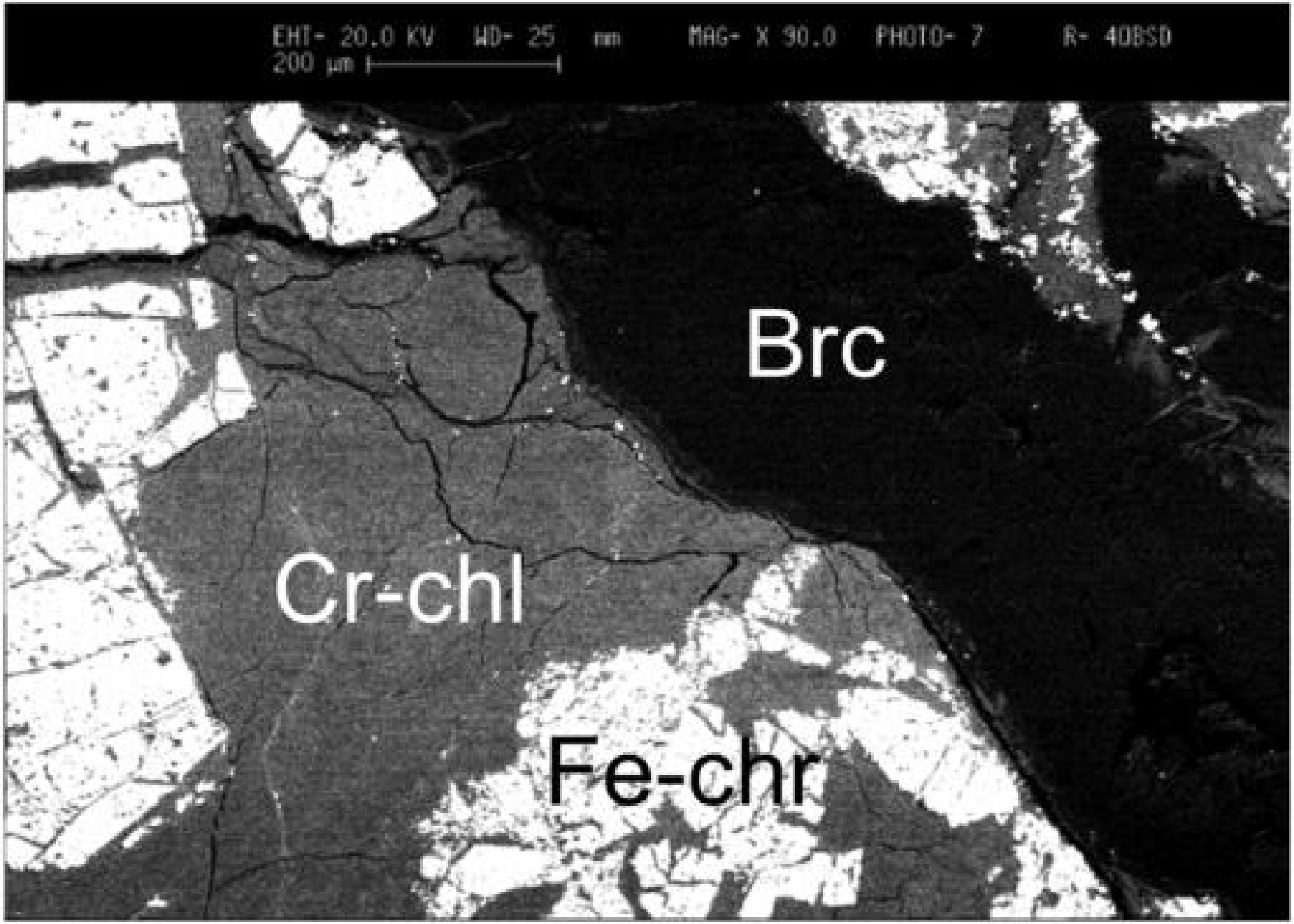
EHT- 20.0 KV WD- 25 mm MAG- X 90.0 PHOTO- 7 R- 40BSD
200 µm
Brc
Cr-chl
Fe-chr

Figure 2

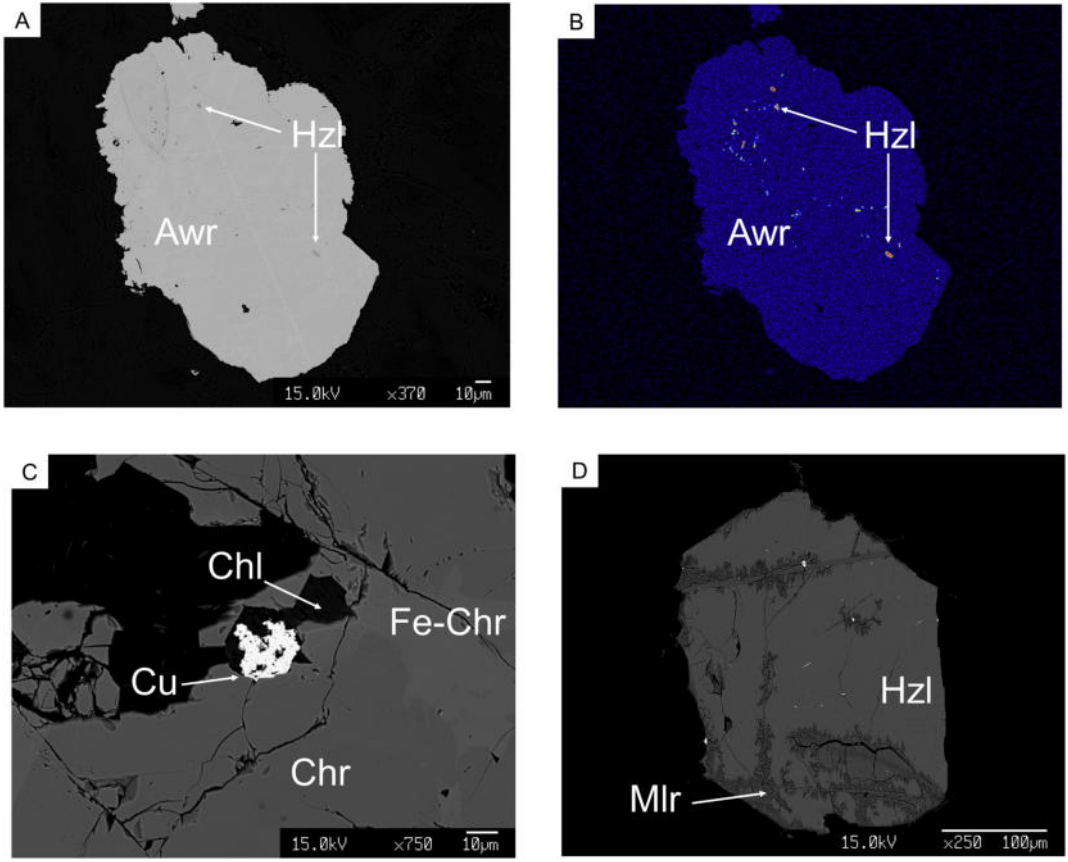
A
Hzl
Awr
15.0kV ×370 10µm
B
Hzl
Awr
C
Chl
Fe-Chr
Cu
Chr
15.0kV ×750 10µm
D
Hzl
Mlr
15.0kV ×250 100µm

Figure 3

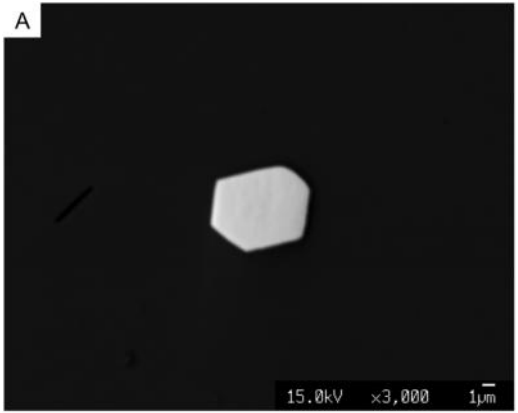
A
15.0kV ×3,000 1μm

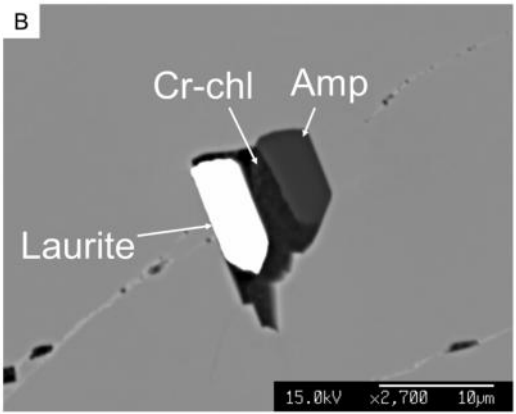
B
Cr-chl
Amp
Laurite
15.0kV ×2,700 10μm

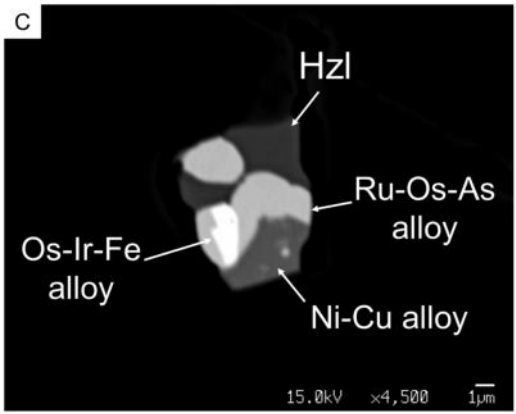
C
Hzl
Ru-Os-As alloy
Os-Ir-Fe alloy
Ni-Cu alloy
15.0kV ×4,500 1μm

Figure 4

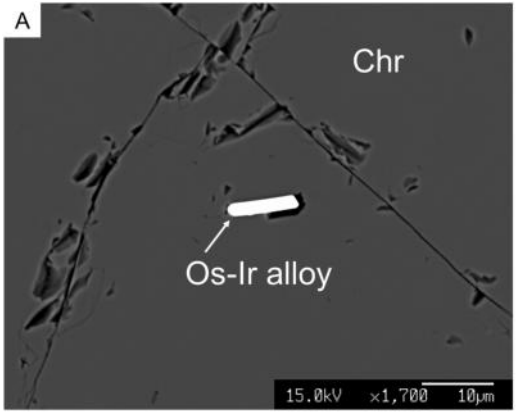
A
Chr
Os-Ir alloy
15.0kV ×1,700 10µm

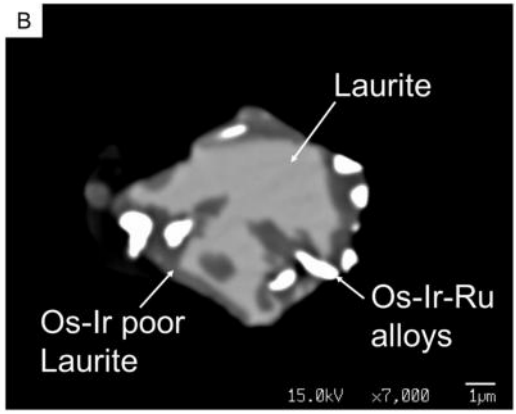
B
Laurite
Os-Ir poor
Laurite
Os-Ir-Ru
alloys
15.0kV ×7,000 1µm

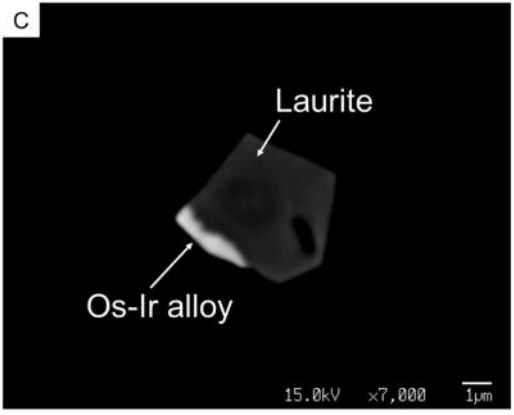
C
Laurite
Os-Ir alloy
15.0kV ×7,000 1µm

Figure 5

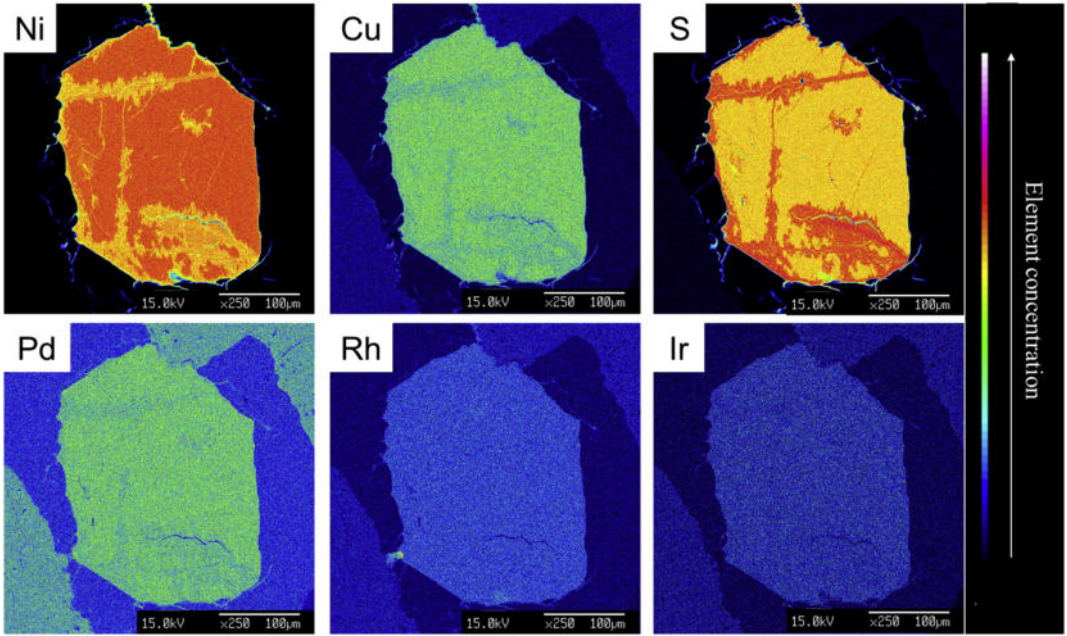

Figure 6

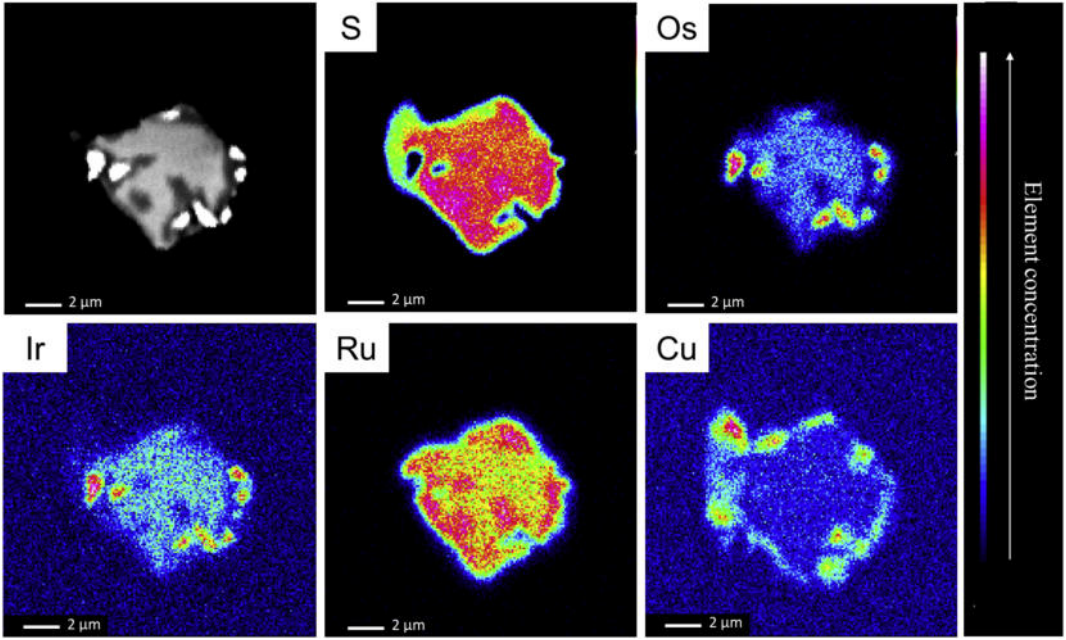

Figure 7

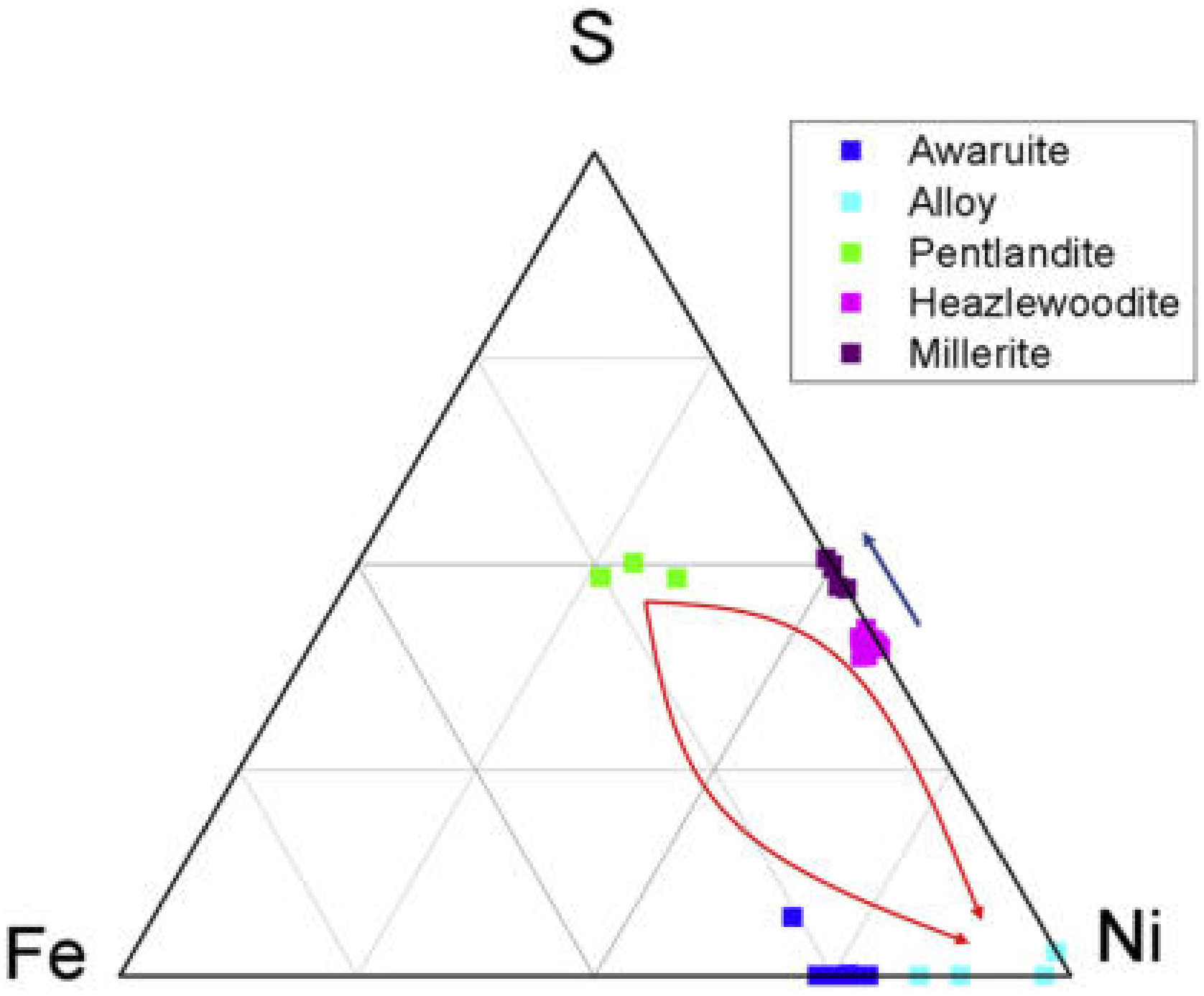
S
Awaruite
Alloy
Pentlandite
Heazlewoodite
Millerite
Fe
Ni

Figure 8

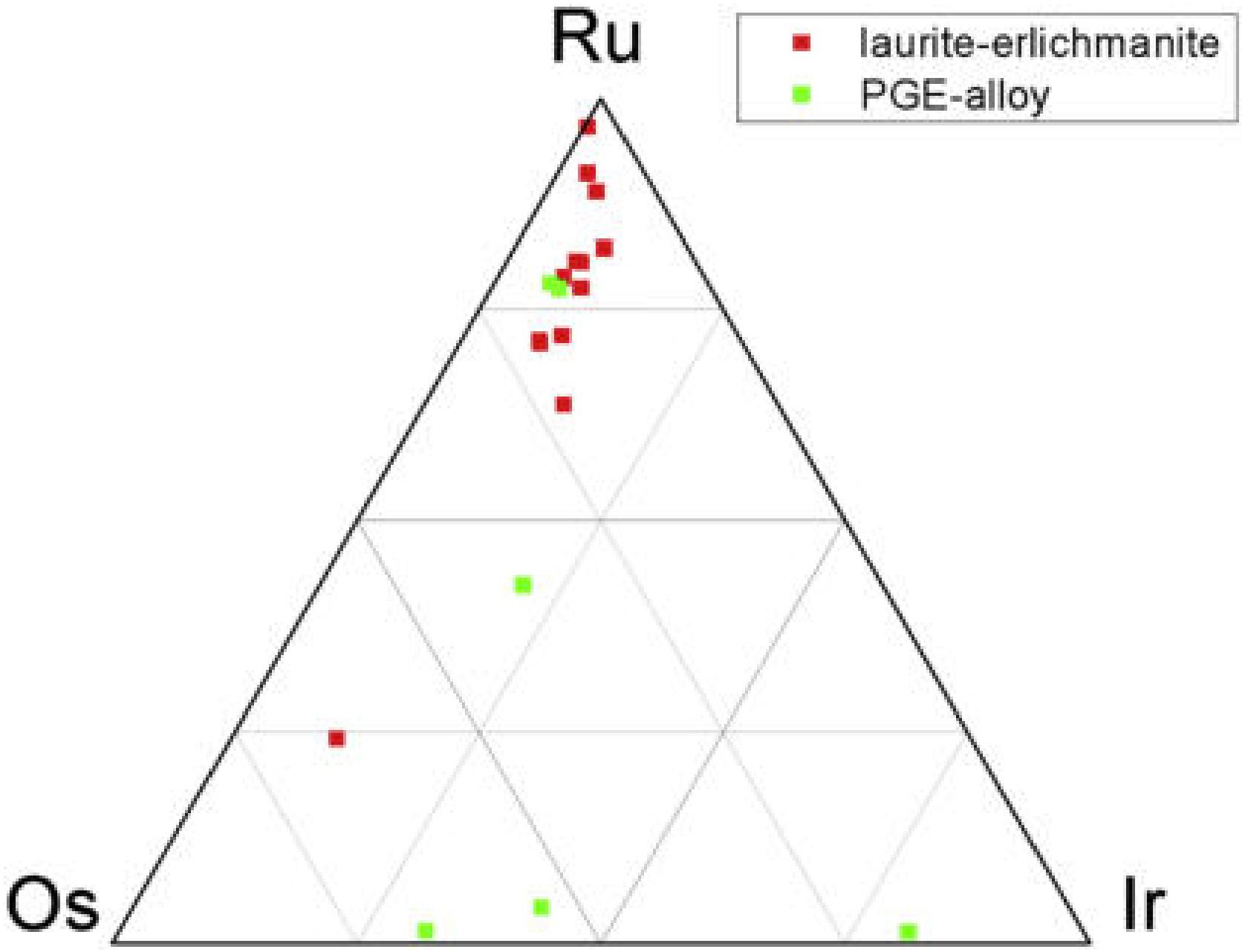

Figure 9

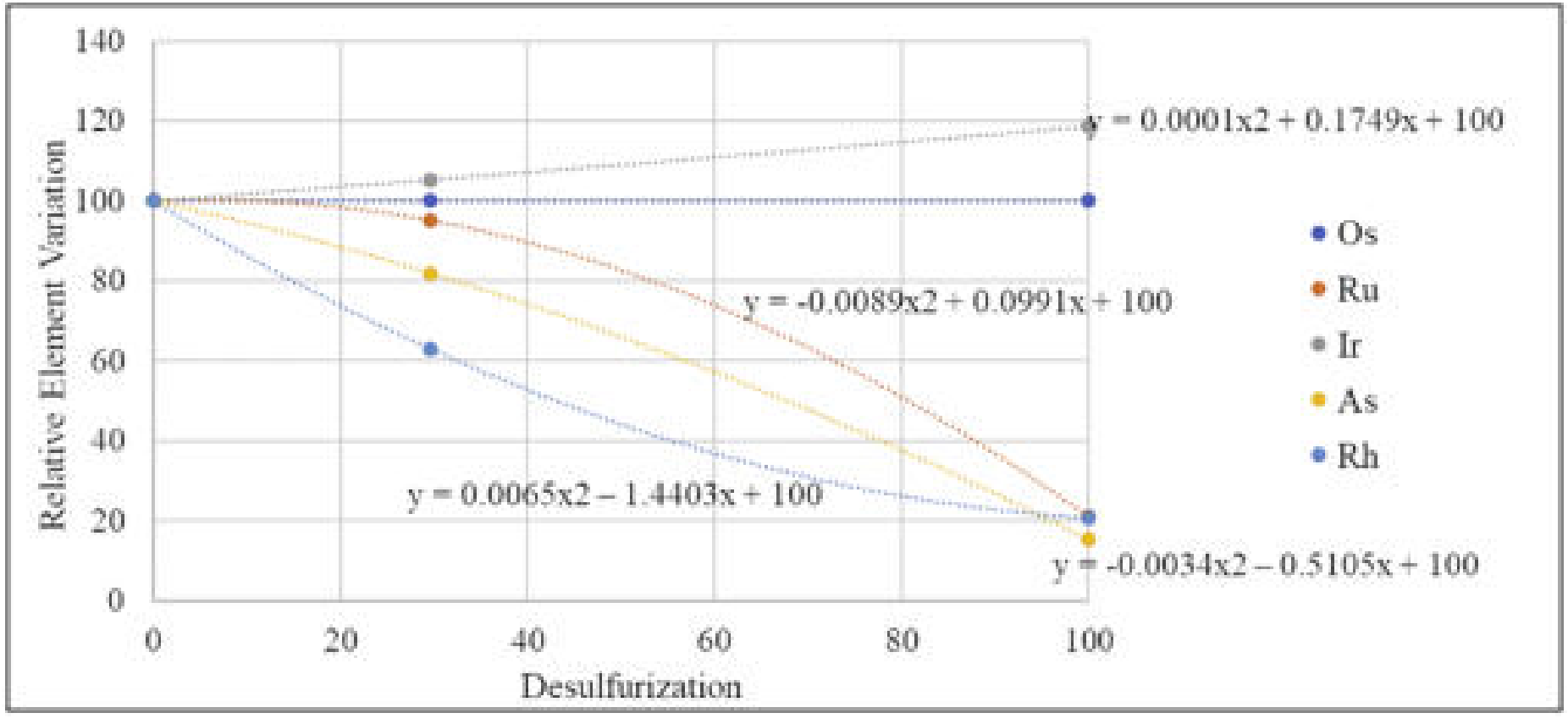
140
120
100
80
60
40
20
0
Relative Element Variation
0
20
40
60
80
100
Desulfurization
y = 0.0001x2 + 0.1749x + 100
y = -0.0089x2 + 0.0991x + 100
y = 0.0065x2 – 1.4403x + 100
y = -0.0034x2 – 0.5105x + 100
Os
Ru
Ir
As
Rh

Figure 10

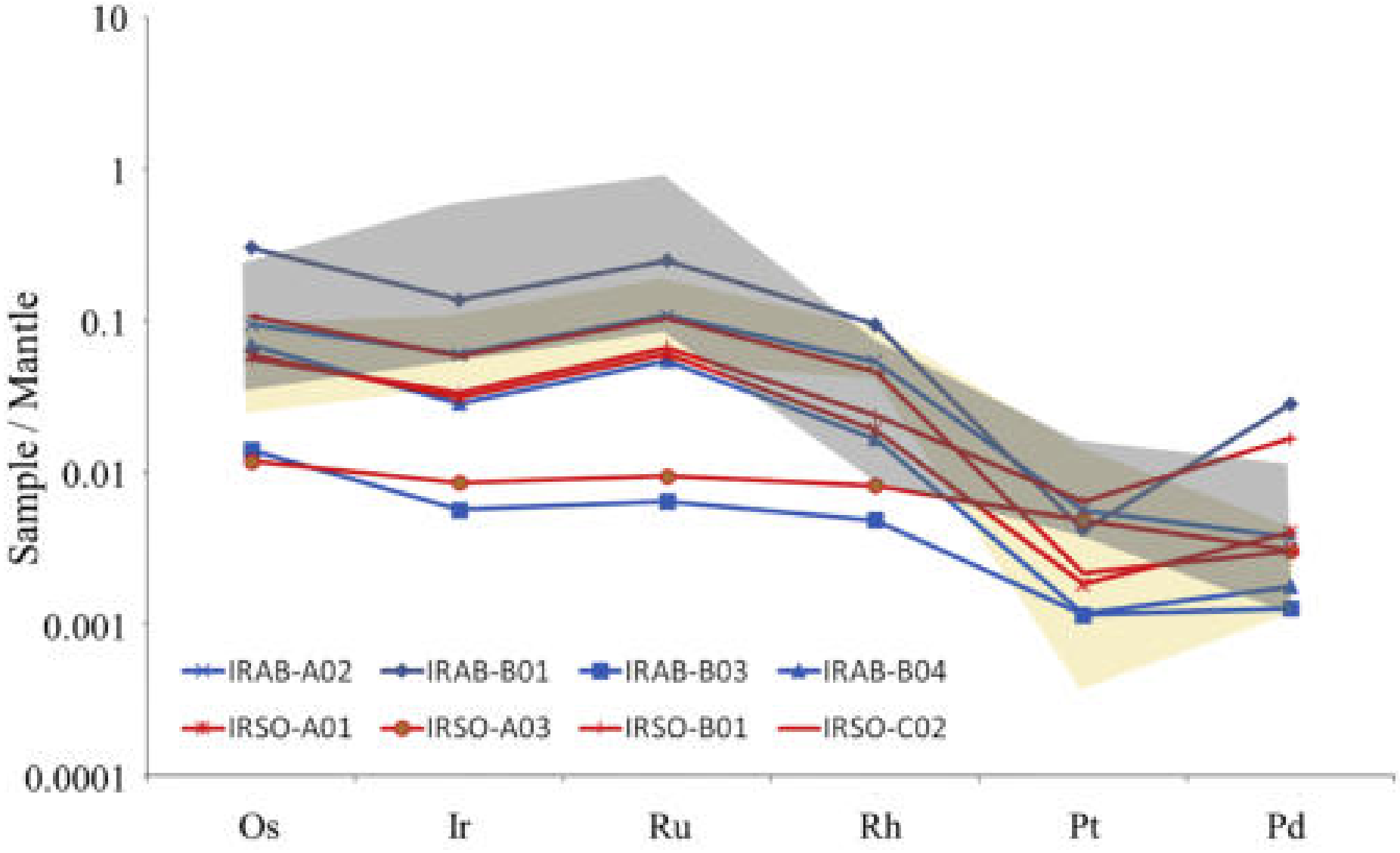
10
1
0.1
0.01
0.001
0.0001
Sample / Mantle
IRAB-A02
IRAB-B01
IRAB-B03
IRAB-B04
IRSO-A01
IRSO-A03
IRSO-B01
IRSO-C02
Os
Ir
Ru
Rh
Pt
Pd

Figure 11

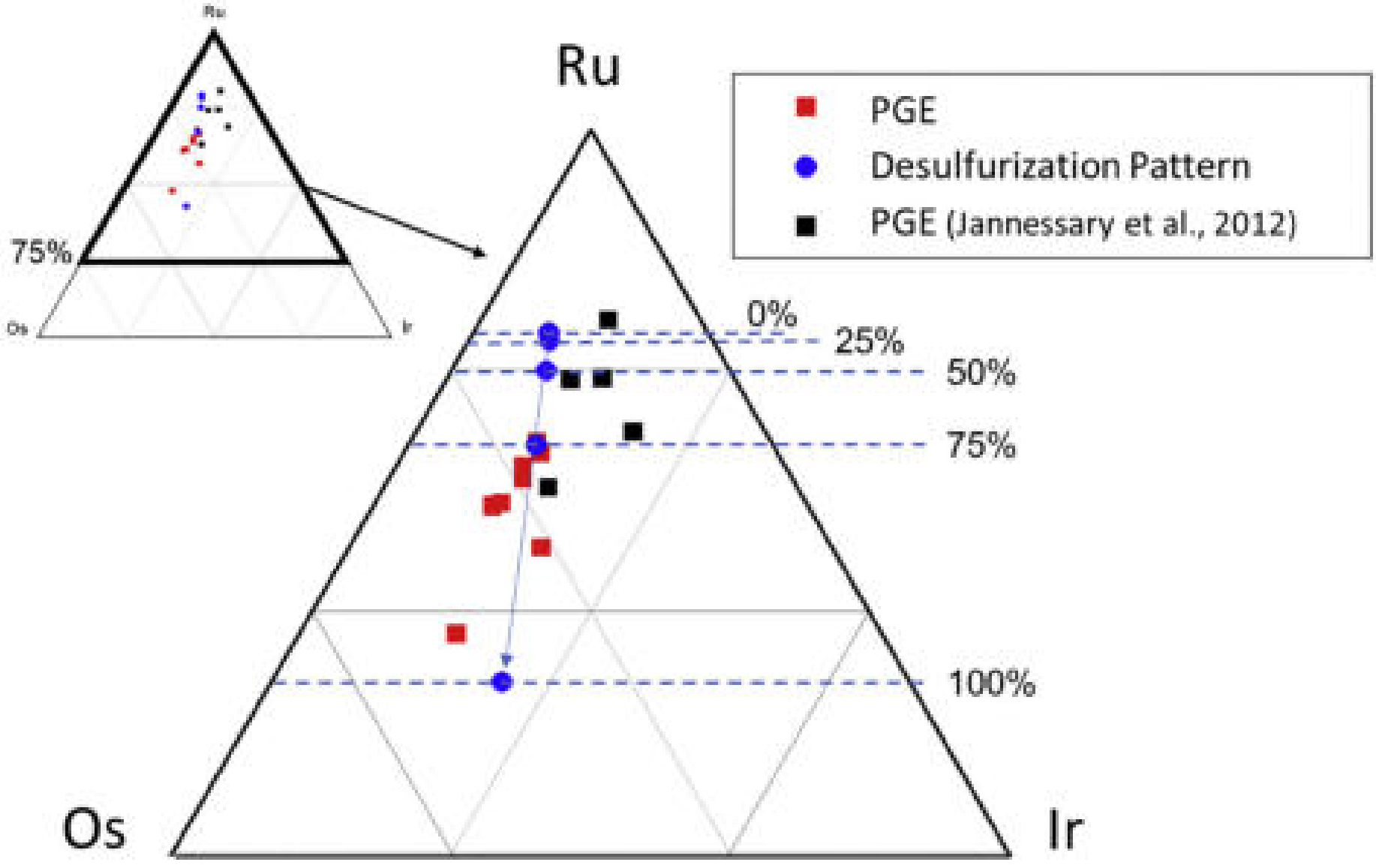
Ru
75%
Os
Ir
Ru
PGE
Desulfurization Pattern
PGE (Jannessary et al., 2012)
0%
25%
50%
75%
100%
Os
Ir

Figure 12

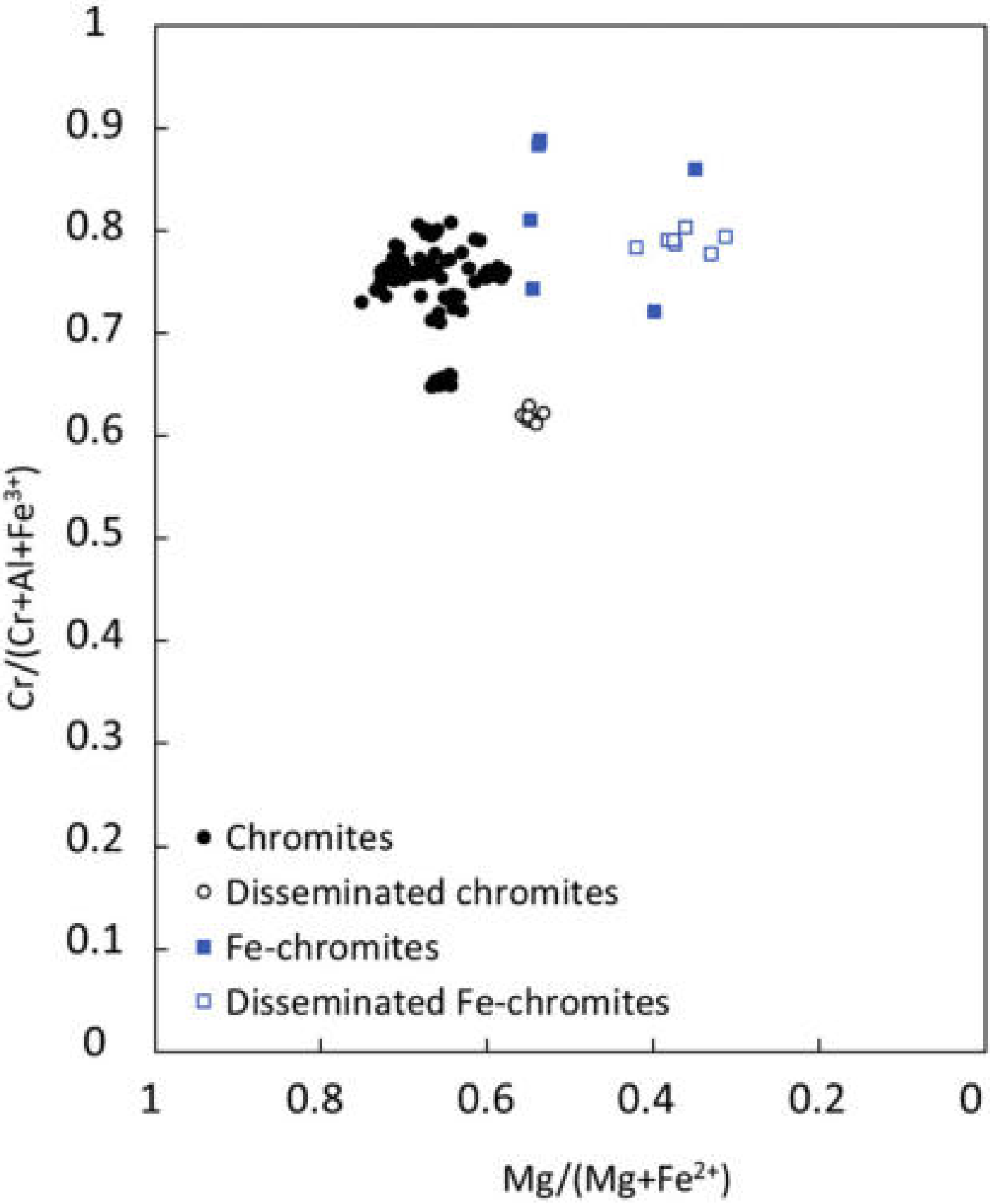
1
0.9
0.8
0.7
0.6
0.5
0.4
0.3
0.2
0.1
0
Cr/(Cr+Al+Fe3+)
Chromites
Disseminated chromites
Fe-chromites
Disseminated Fe-chromites
1
0.8
0.6
0.4
0.2
0
Mg/(Mg+Fe2+)

Figure 13